Bulletin of Earthquake Engineering
https://doi.org/10.1007/s10518-024-01895-z

ORIGINAL ARTICLE

Dynamic identification and seismic capacity of an innovative cleanroom with walkable ceiling system

Gennaro Magliulo[1,2] · **Martino Zito**[1] · **Danilo D'Angela**[1]

Received: 16 October 2023 / Accepted: 7 March 2024

Abstract
Past earthquakes highlighted the vulnerability of cleanrooms, especially in earthquake-prone countries like Italy; the post-earthquake reconnaissance showed that damage to cleanrooms led to immeasurable economic losses. This study investigates the seismic performance of an innovative cleanroom, seismically designed and provided with innovative components. Full-scale shake table tests were performed on the cleanroom according to ICC-ES AC156 protocol; the cleanroom was tested under operating conditions. Both dynamic properties and seismic behavior of the specimen were assessed. The tests showed the excellent seismic behavior of the cleanroom, confirming that simple devices can significantly improve the seismic performance of nonstructural elements.

Keywords Nonstructural elements · Cleanroom · Shake table test · Dynamic identification · Seismic performance · Earthquake engineering

1 Introduction

Cleanroom or white room is an enclosed engineered space/facility having a controlled environment in terms of airborne particles, pressure, relative humidity, and temperature, required to perform specific production and treatment activities that need a strictly-controlled environment (European Committee for Standardization (CEN) 2021; Liu et al. 2021; Yang et al. 2021). Cleanrooms are widely used in pharmaceutical, food, and electronic manufacturing industries (Loomans et al. 2020; Shao et al. 2022; Zhang et al. 2022) and in healthcare and hospital facilities (e.g., operating theater) (Andersson et al. 2012; Can et al. 2021).

Cleanrooms can be classified as nonstructural elements (NEs) (Braga et al. 2011; Federal Emergency Management Agency (FEMA) 2012; Soroushian et al. 2016; Taghavi and Miranda 2003; Yang et al. 2023) since they are not part of the structural system of buildings and facilities; however, they are very peculiar NEs since they consist in complex

✉ Gennaro Magliulo
gmagliul@unina.it

[1] Department of Structures for Engineering and Architecture, University of Naples Federico II, Via Claudio, 21, 80125 Naples, Italy

[2] Construction Technologies Institute (ITC), National Research Council (CNR), 80125 Naples, Italy

Published online: 13 March 2024

architectural systems integrating mechanical, electrical, electronic, and hydraulic facilities and equipment (American Society of Civil Engineers 2017; Federal Emergency Management Agency (FEMA) 2012). Cleanrooms are often highly vulnerable and exposed to damage caused by seismic actions, as highlighted by the 2012 Emilia earthquake (Petruzzelli 2016). In particular, the cleanroom partitions exhibited major seismic damage, such as cracking and collapse of plaster panels and failure of ceiling-mounted equipment. This response caused significant damage to room's content and required major restoration intervention in terms of facilities and equipment prior to reinstate the production. Therefore, seismic damage of cleanrooms can threaten life safety and can cause severe economic losses due to property loss and downtime (Federal Emergency Management Agency (FEMA) 2012; Taghavi and Miranda 2003). For example, microchip manufacturing equipment used in electronic manufacturing facilities is extremely valuable, and total cost of NEs can even be higher than 97% of the total cost of semiconductor fabrication plants (Hwang et al. 2007). Furthermore, as NEs, cleanrooms are not typically designed considering seismic actions, and relatively frequent earthquakes might even cause significant losses and functioning disruption, which are extremely critical for production and manufacturing facilities.

In the last few decades, several studies investigated architectural NEs such as partitions and ceiling systems (Arifin et al. 2020; Magliulo et al. 2012; Mulligan et al. 2020; Perrone et al. 2020; Petrone et al. 2017; Soroushian et al. 2015), as well as a growing literature focused on electrical/mechanical/hydraulic equipment and components (Blasi et al. 2018; Butenweg et al. 2021; Ghalibafian et al. 2004; Tian et al. 2015; Tran et al. 2020), and free-standing elements housed within critical facilities (D'Angela et al. 2022; Di Sarno et al. 2019; Filiatrault et al. 2004; Prota et al. 2022; Wittich and Hutchinson 2015). However, to the authors' knowledge, no studies focused on the seismic performance of complex NEs that integrate architectural and electrical, electronic, mechanical, and hydraulic systems, especially under functioning conditions, such as cleanrooms. Despite the recent research advances towards a reliable seismic assessment and an effective protection of critical systems and components, dynamic properties and seismic vulnerability of cleanrooms is still unknown, and this results in a critical knowledge gap, as well as it is associated with critical seismic risk.

The present study represents a first step carried out to address the abovementioned research gap, i.e., an experimental investigation on the seismic performance of a full-scale cleanroom with a walkable ceiling system, by means of shake table tests. Traditional cleanrooms do not typically present seismically designed connection systems among the different components, and, in some cases, the connections or structural details are insufficient, and the lateral partition system has independent behavior. Under seismic actions, this configuration can result in local collapse mechanisms and thus the cleanroom exhibits high seismic vulnerability. The cleanroom was designed to replicate typical construction practice and technology according to compliant codes, also implementing construction solutions to maximize the seismic performance; the documental compliance reference is associated with ISO Class 7 (European Committee for Standardization (CEN) 2021). A cleanroom differs from an ordinary ventilated room in some ways: (a) increased air supply, (b) high-efficiency filters (e.g., high-efficiency particle air (HEPA) filters, or ultra-low particle air (ULPA) filters), (c) terminal air filters, (d) room pressurization and pass-through grilles. Another peculiarity of a cleanroom is the type of surface finish in the room.

The tests were carried out under full functioning conditions, including ventilation, air conditioning, pressure, and electronic opening control. Both dynamic identification and seismic performance evaluation tests were carried out according to ICC-ES AC156

protocol (International Code Council Evaluation Service (ICC-ES) 2020). The tests represent a seismic qualification of the designed cleanroom (Filiatrault et al. 2021; Merino et al. 2023; Zito et al. 2022b, 2022a). Seismic qualification is discussed in an extensive and technical manner in recent literature studies (Merino et al. 2023; Zito et al. 2022b). This method represents the most robust and comprehensive option for seismically assess and qualify NEs, but it is not exempt from limitations, as it was discussed by Merino et al. (2023). As a matter of fact, the seismic qualification relies on the assumption that the qualification input is representative of seismic scenarios, in terms of seismic characteristics and damage potential. However, recent studies highlighted that current shake table testing protocols might not be necessarily reliable for peculiar applications (D'Angela et al. 2022). Furthermore, in order to be robust and reliable, the qualification testing setup should be consistent with actual (or realistic) arrangements of NEs, even considering the boundary conditions and the potential interaction with other systems. Therefore, the qualification results reported in this study, albeit representing the state-of-the-art, should be carefully interpreted and referred to the specific application.

2 Methodology

2.1 Experimental facilities and testing setup

Shake table tests of an innovative cleanroom in real scale were carried out at the laboratory of the Department of Structures for Engineering and Architecture of the University of Naples Federico II, Italy. The tests approximately simulated the representative seismic response of a cleanroom installed within a building. The shake table has a 3×3 m plan dimension and a total height of 1.45 m. It has two (horizontal) degrees of freedom and a maximum payload equal to 200 kN, with an operation frequency range of 0–50 Hz, peak acceleration equal to 1 g (maximum payload), peak velocity equal to 1 m/s, and a stroke equal to 500 mm (± 250 mm) (Magliulo et al. 2014). The testing setup was defined in order to replicate a realistic and typical arrangement of the cleanroom within the hosting facility, with particular attention to the functioning/service facilities/systems. It should be recalled that cleanrooms are fixed at their bases to building floors, and they are often located at lower floors of low- or mid-rise buildings. The height of cleanrooms is typically lower than the hosting inter-story height, and a plenum space of variable height (ranging from 40 to 400 cm) is typically arranged between the top of the cleanroom and the upper floor of the building. Most functioning facilities and equipment (e.g., pipeline and electrical networks) are located within this plenum space and connect the external supply to the cleanroom, according to the functioning conditions of the cleanroom.

The shake table was representative of a building floor for installation of the cleanroom, even though, as it discussed in the following, the setup is not fully consistent with the realistic seismic behavior of the cleanroom-building system (e.g., Zou et al. 2023). In the following, shake table response is meant as a floor response, and peak table accelerations (PTA) are meant as peak floor accelerations (PFA); in particular, a wood slab was used as an interface between the shake table and the cleanroom. The base constraints used in the study are compatible with the actual arrangements of cleanrooms within reinforced concrete structures and the presence of the wood slab did not affect the response of the cleanroom at all, as it will be discussed in the following sections. A steel test frame was designed and constructed to support the plenum space facilities and the ceiling of the cleanroom.

The test frame base was fixed to the floor of the testing lab and was not subjected to loading conditions. Figure 1 shows the testing setup and the side views.

In realistic seismic scenarios, while the base of the cleanroom would be subjected to the i^{th} building floor motion, the constraints of the ceiling suspension devices would be subjected to the motion of the $(i+1)^{th}$ building floor. This condition could have been achieved by installing a special test frame on the shake table, connecting its top to the ceiling system of the cleanroom; the test frame would have been designed to transfer the shake table's actions (i^{th} building floor) to the ceiling in order to replicate, at the frame top, the response of a realistic $(i+1)^{th}$ building floor, in terms of both accelerations and displacements (e.g., Petrone et al. 2017). Given the large dimensions of the cleanroom, there was not space on the shake table to install the test frame, and this had to be fixed to the laboratory floor, outside the shake table. However, this testing condition did not affect the significance of the relative displacement assessed between the cleanroom ceiling and the frame top, as it is also discussed further in the following.

The steel test frame was designed according to Eurocode 8 (British Standards Institution and European Committee for Standardization 2005) and Italian building code NTC 2018 (Ministero delle Infrastrutture e dei Trasporti 2018). Design loads consisted of dead loads related to ceiling (0.3 kN/m^2) and pipeline (0.2 kN/m^2) and horizontal load equal to 1.0 kN/m^2. Furthermore, due to the probability of overturning of the panels of the cleanroom, or even the entire specimen, some beam stumps were designed and connected through ropes locked with a spring catch. The designed frame consisted in a spatial steel moment-resisting frame (MRF) structure with layout dimensions of 2.60 m (Y direction) × 6.21 m

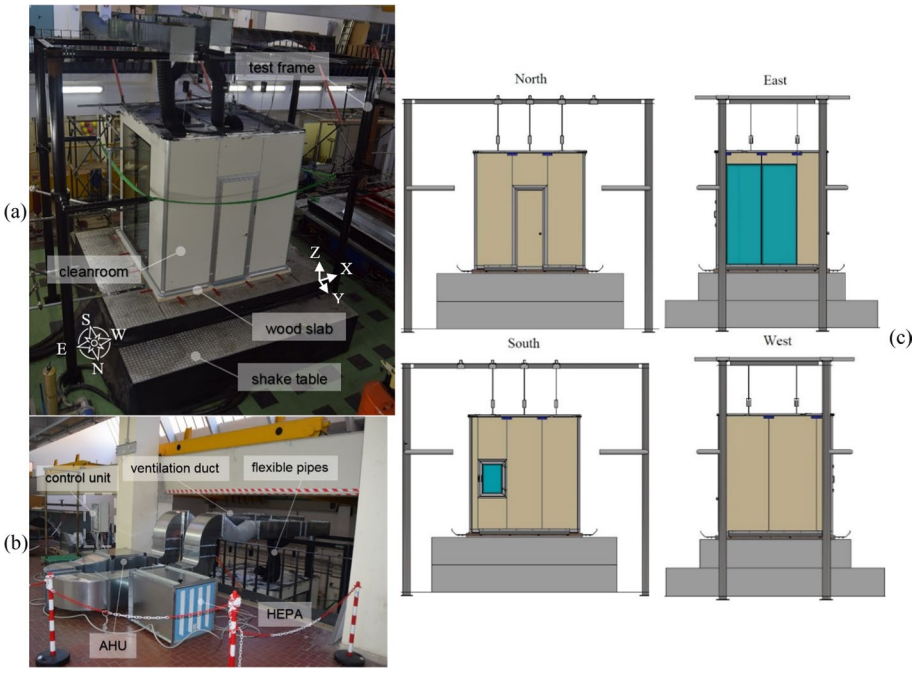

Fig. 1 Testing setup: **a** global view, **b** perspective views, and **c** centralized heating, ventilation, and air conditioning (HVAC) filtration system and control unit

(X direction) × 6.00 m (Z direction). The structure consisted of S355JR circular hollow section (CHS) 193.7 × 10 mm columns, S275JR HEA 120 mm primary beams, and S235JR rectangular hollow section (RHS) 9 × 50 × 3 mm secondary beams. The primary to secondary beam connection was achieved through tie type fastening using class 8.8 M12 bolts. The primary beam to column connections were bolted with bolted cover plate splices (moment-resisting connection), and the column to floor connections were bolted through welded base plate. A finite element (FE) model of the test frame was defined in PROSAP (2S.I. Software e Servizi per l'Ingegneria S.r.l. 2020). In particular, the frame members were modeled as elastic *beam elements*. The natural vibration periods of the frame were assessed, and the two first translational periods resulted in 0.300 s (3.33 Hz) along X direction and 0.289 s (3.45 Hz) along Y direction.

The cleanroom was connected to the shake table through a wood slab (Fig. 1a) since this was associated with a clean, rapid, and low-cost installation/transportation condition that was also relatively conservative in terms of connection response. The presence of the wood slab did not condition the seismic response of the cleanroom, and this is discussed in terms of recorded acceleration in the following sections. The wood slab was composed of two layers of poplar plywood, and each layer had a thickness of 35 mm and dimensions of 3 × 3 m. The total weight of the wood slab was about 3.92 kN. To achieve higher stiffness and strength in the slab plane, the two layers were installed perpendicularly to each other, in terms of resisting fiber directions. The wood slab was connected to the shake table by equidistant bolts, tightened with controlled torque.

The tested cleanroom is classified according to UNI EN ISO 14644-1 (European Committee for Standardization (CEN) 2021) of ISO Class 7. This cleanroom class filtration system must provide filter coverage of 15–25% and a minimum of 60 air changes per hour (ACH) (European Committee for Standardization (CEN) 2021). Equivalently, the tested cleanroom is classified as grade C according to good manufacturing practices (European Commission 2010).

The tested cleanroom is known as turbulently-ventilated or nonunidirectional flow, the air being supplied by air supply diffusers or filters in the ceiling similar to that found in offices, shops, etc.

Electrical and ventilation systems were installed and made fully operative during the tests to recreate the functioning condition of the cleanroom in realistic conditions (i.e., serviceability) (British Standards Institution and European Committee for Standardization 2005). In particular, a centralized heating, ventilation, and air conditioning (HVAC) filtration system and a control unit implement the functioning conditions of the cleanroom (Fig. 1c), also including an air handling unit (AHU system) provided with high-efficiency particulate air filters (HEPA), a galvanized sheet metal piping system, necessary to circulate air, cleanroom supplies and sensors (pressure control). The system was able to keep the pressure in the cleanroom constantly equal to at about 40 Pascal, with tolerance of ± 5%, so as to ensure an ISO class of air cleanliness of ISO Class 7 according to the relevant requirements (European Committee for Standardization (CEN) 2021; Yang et al. 2021). The electrical system consisted of a control unit for the operation of the cleanroom opening system, internal pressure sensor, and lighting system. The opening system includes a door and a pass-box, often referred to as pass-through hatch. Both service units were placed in an external area that was isolated from the shake table area, and the related network system was realized through a duct system, flexible pipes, and cable trays. The network system was realized favoring flexible connections among the different components, in order to minimize the transfer of the dynamic actions and the associated deformations from the cleanroom to the units.

The locks of the cleanroom openings (door and pass-box) were electrically controlled in terms of "on" and "off" locking conditions by the central locking system and via an opening keypad, located next to the door; in particular, prior to opening a lock due to a key command, the locking system locks the other one: this is aimed at preventing sudden drops in pressure inside the cleanroom and minimizing the potential contamination of the internal environment. The unlocked/locked condition of the opening is displayed through green/red led lights.

2.2 Cleanroom specimen

The specimen was a real-scale cleanroom consisting in the assembly of base/flooring, lateral partition system, ceiling, and electric/ventilation facilities. The plan dimensions of the cleanroom are about 2.8×2.8 m, while its height is about 3.0 m. The dimensions of the specimen are representative of a typical cleanroom used within food, pharmaceutical and healthcare facilities. In the following, the main components of the cleanroom are described, and the mounting procedure is briefly reported. The geometrical details of the elements and the technical specificities of the assembly are omitted for the sake of brevity since they are available within the technical reports (Magliulo 2021). The cleanroom system development was based on the implementation of innovative technologies patented by one of the authors (Mangini et al. 2020). A focus on the innovative technologies and devices is reported in Sect. 2.3. The overall weight of the cleanroom including the weight of the ceiling system (1.96 kN) is 13.4 kN. The definition of the cleanroom system follows. The base layout of the cleanroom was composed by an assembly of extruded aluminum 6060-T5 elements, i.e., stiffened rectangular cross-section profiles (Fig. 2a(1)), flanged floor rail profiles (Fig. 2a(2)), and angular bracket profile elements (Fig. 2a(3)). Moreover, three innovative components of S275 steel material were introduced: bottom splice (Fig. 2a(4)), bottom block (Fig. 2a(5)), and bottom block with thread rod (Fig. 2a(6)); in particular, these components were designed to connect base layout components to the overall cleanroom and improve its seismic performance. The base layout of the cleanroom is shown in Fig. 2a(7). The rectangular profiles were fastened to the wood slab with screws passing through fitted holes (Fig. 2a(8)); these profiles defined the plan layout of the cleanroom, i.e., external cleanroom walls and pass-box/airhole internal cavities (Fig. 2a(7)). The floor rail profiles were installed on the rectangular profiles and were screw fastened to them along both lateral surfaces; angular bracket elements were screw fastened to both profiles and wood slab (Fig. 2a(9)). The connection between the rectangular profiles corresponding to corners of both cleanroom walls and pass-box/airhole elements was implemented by the bottom splice (Fig. 2a(10)). The bottom block was installed to connect the base of the cleanroom to the vertical splice profiles of the panels of the walls, described in the following subsection. In particular, the bottom block was inserted into the slot of the telescoping track, then fixed with a clamp and, finally, fastened to the vertical splice profiles by bolts (Fig. 2a(11)). When it was not possible to install the vertical splice profile between the panels, i.e., as for the environment of the pass-box, the bottom block was connected with a threaded rod through a bolt (Fig. 2a(12)).

The lateral partition system included blind and transparent panels, openings (door and pass-box), and various assembly and connection components (Fig. 1). The lateral partition assembly also included cavities, i.e., the functioning chamber of the pass-box, blind cavities below and above the pass-box, and airhole cavity. The main components of the lateral partition system consist of blind metal panels, transparent (metal–glass)

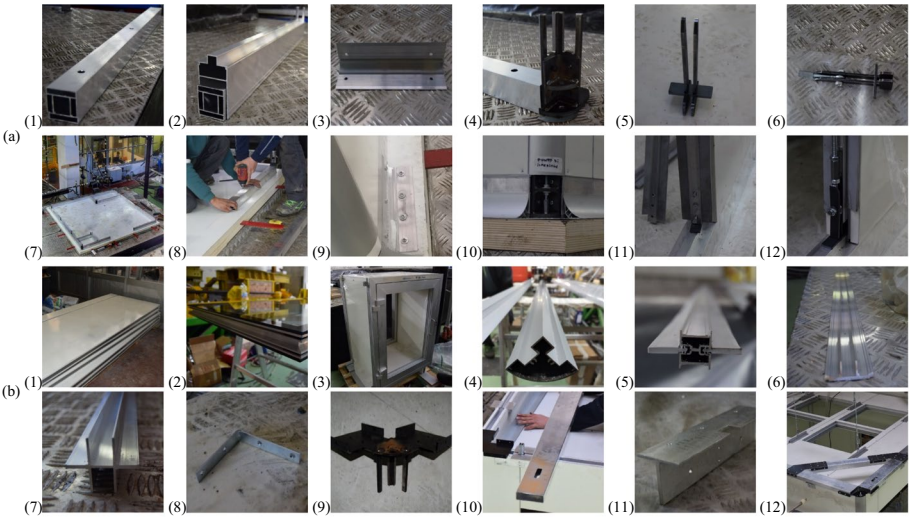

Fig. 2 Details of cleanroom components; **a** base layout: (1) stiffened rectangular cross-section profile, (2) flanged floor rail profiles, (3) angular bracket profile element, (4) bottom splice, (5) bottom block, (6) bottom block with thread rod, (7) base layout, (8) rectangular profile to wood screw fastening, (9) floor rail (and rectangular) profile(s) to wood slab screw fastening using angular bracket element, (10) detail of the bottom splice connection, (11) fastened to the vertical splice profiles, and (12) connected with a threaded rod; **b** lateral partition system: (1) blind metal panels, (2) transparent (metal–glass) panels, (3) pass-box chamber, (4) curved angular profiles, (5) (vertical) splice profiles, (6) π-shaped profiles, (7) H-shaped profiles, (8) single bracket elements, (9) top splice, (10) RHS profile, (11) T-profile, and (12) horizontal brace

panels, door (and framing), pass-box, and several assembly/construction profiles and elements (i.e., curved angular profiles, (vertical) splice profiles, angular bracket profile elements, π-shaped and H-shaped profiles, single bracket elements, and shell profiles). Moreover, some innovative components were designed and installed to prevent seismic local collapse mechanisms. The main components and innovative components of the lateral partition system of the cleanroom are depicted in Figs. 2b and 3a. All full-height panels of the cleanroom except openings (door, pass-box, transparent panels) consisted of blind panels. The blind panels (Fig. 2b(1)) were made by the assembly of two stainless prepainted steel layers on an aluminum frame, with an infilled insulation layer.

The aluminum frame of the panels corresponded to the external perimeter of the panels and was infilled within the panel layers; the corners of the aluminum frame profiles were connected and stiffened by internal brackets. The steel layers were bonded to the insulation through a two-part polyurethane adhesives cure (2C PUR). The panels have a total thickness of 62 mm and a weight of 0.24 kN/m^2.

Two identical full-height panels included within the east side of the cleanroom (east view, Fig. 1b) consisted of assemblies of a transparent and a blind panel. Transparent (metal–glass) panels (Fig. 2b(2)) covered the majority of the full height from the base of the cleanroom, and blind panels were located on the top of them. Transparent panels were made of two layers of laminated glass, glued to an infilled perimetrical aluminum frame, in a configuration similar to the metal panels' one. The openings of the cleanroom consisted of a door and a pass-box (Fig. 2b(3)). The partition panel with the door (north view, Fig. 1a) was composed of an aluminum hinged door and a blind panel

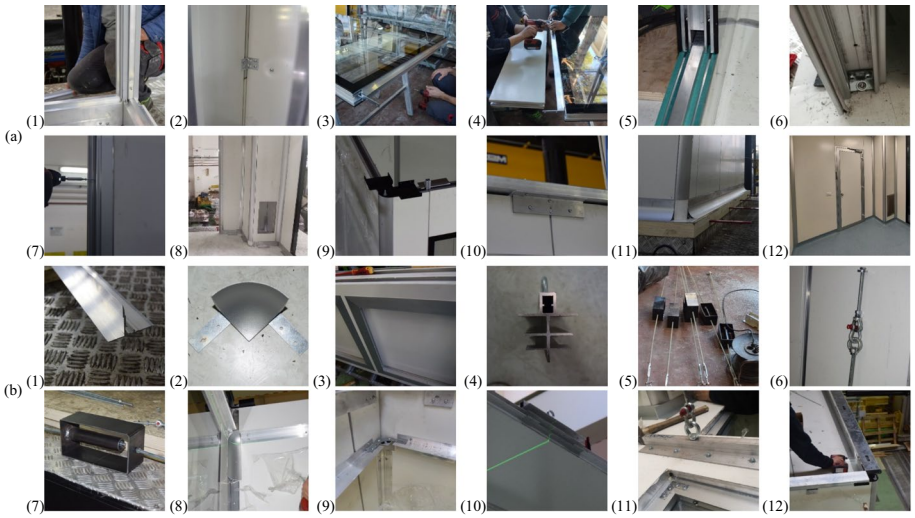

Fig. 3 Details of cleanroom components; **a** lateral partition system: (1) curved angle and splice profiles assembly, (2) perpendicular blind panels bracket fastening, transparent to blind panels connection: (3) H-shaped profile and brackets and (4) panels' assembly, (5) shock absorber on floor rail profile, (6) bracket connecting door frame base to wood slab and adjacent panels, (7) door frame screw fastening, (8) airhole, (9) detail of the top splice connection, (10) detail of the T-profile connection, (11) shell profiles, and (12) internal floor of the cleanroom; **b** ceiling system: (1) T-shape profiles, (2) angular joint connector, (3) load-bearing panels, (4) stiffened suspension connection profile elements, (5) hanger-suspension devices, (6) detail of (superior) hinge device (suspension), (7) detail of spring device (suspension), (8) fastening of the T-shape profiles to the vertical panels, (9) adjacent perpendicular T-shape profile fastening through angular joint connectors, (10) detail of connection among panel, H-shaped profile, and stiffened suspension connection profile element, (11) fastening of stiffened suspension connection profile elements to panels, and (12) fastening of angular profile elements to vertical panels

located above the door. The partition section hosting the pass-box (south view, Fig. 1c) was composed of a three-dimensional assembly of blind panels defining the cavity in which the (pre-assembled) pass-box chamber was inserted and the construction cavities (below and above the pass-box). The pass-box chamber was delimited by internal and external openings (i.e., pass-box windows).

The curved angular profiles (Fig. 2b(4)) were installed at the corners of the perpendicular lateral panels and at the corners of the pass-box and airhole panels, two splice profiles (Fig. 2b(5)) were prearranged within the slots of each curved profile, as shown in Fig. 3a(1); in particular, each vertical splice profile was screw fastened to the curved profile along the height. The panels were connected to the corner vertical splice profiles and were located/arranged along the cleanroom base layout. 4 mm-width gaps were arranged between adjacent in-line panels, and vertical splice profiles provided with two gaskets were placed within these gaps; this arrangement was aimed at favoring rapid and economic rearrangement/replacement of the panels. Adjacent perpendicular panels corresponding to pass-box were screw fastened using angular bracket profile elements (Fig. 3a(2)). The corner panels of the cleanroom and the pass-box/airhole internal panels were screw fastened to the flange of the floor rail profiles.

Pass-box was installed on the south side of the cleanroom (Fig. 1b) after the insertion cavity was arranged; in particular, blind panels were assembled to define the pass-box

boundary cavities (below and above the pass-box chamber). The short blind panels (within the cleanroom perimeter) were screw fastened to the perimeter ones by using π-shaped profiles (Fig. 2b(6)), and these latter profiles were also used to connect the pass-box chamber to the inferior and superior blind panels. Screws and brackets were used to fasten the pass-box chamber to the adjacent panels, as well as perpendicular blind panels were screw fastened through angular bracket profile elements (Fig. 3a(2)).

The two transparent-blind full-height panels (east view, Fig. 1b) were pre-assembled prior to be mounted on the floor rail profiles (Fig. 2a(2)); each metal panel was screw fastened to the transparent panel through a H-shaped profile (along the panels' width, Fig. 2b(7)) and lateral brackets (Fig. 2b(8)) (Fig. 3a(3) and (Fig. 3a(4)). Two layers of shock absorber were attached to the floor rail profiles prior to arranging the transparent-blind panels in order to minimize the damage to the glass panels (Fig. 3a(5)). The adjacent two transparent-blind panels were screw fastened using a vertical H-shaped profile.

The frame of the door (north view, Fig. 1b) was screw fastened to the lateral and top blind panels through π-shaped profiles (Fig. 2b(6)); two small brackets (screws), located at the bases of the frame, were used to connect (screwing) the door frame to the wood slab and to the lateral panels (Fig. 3a(6) and (7)). The door (including the handle) was pre-assembled and was simply hinged to the frame. The airhole (northeast cleanroom corner, Fig. 3a(8)) was defined by lateral blind panels, and π-shaped profiles were used to screw fasten the panels among them; the internal corners related to perpendicular panels were screw fastened (through an angular bracket). HEPA filter was placed at the bottom of the airhole, and a flexible pipe system was screwed and sealed to the top of the airhole to implement the internal-to-external cleanroom airflow.

The bottom splice systems described in the previous subsection were connected to the innovative component placed inside the curved angular profile, referred to here as the top splice (Fig. 2b(9)); in particular, the top splice systems were fastened to the bottom splice systems by a threaded rod (Fig. 3a(9)). Along the upper perimeter of the partition walls of the cleanroom, an aluminum RHS profile was installed (Fig. 2b(10)) and each end of the RHS profiles was fastened to the top edge splice through screws. Moreover, aluminum T-profiles (Fig. 2b(11)) were fixed with screws both inside and outside the partition walls to connect the side-by-side panels of the walls of the cleanroom, the vertical splice profiles, and the RHS profile (Fig. 3a(10)). Finally, horizontal braces were installed on the four top corners of the walls of the cleanroom (Fig. 2b(12)), consisting of an aluminum RHS profile and two 45° plate; the latter was needed to connect by screws the horizontal brace to the RHS profile.

Shell profiles were fixed corresponding to both internal and external cleanroom base perimeter defined by the flooring to lateral partition interfaces (Fig. 3a(11)). These profiles were used for both architectural/aesthetic and technological purposes, in particular, they favor laminar airflow within the cleanroom, minimizing the airflow turbulence. The shell profiles were fixed to the angular profile elements by using silicone sealant. All interfaces between panels and other components were fully sealed by silicone sealant to prevent air pressure loss in the cleanroom. The floor finishing covered all internal floor of the cleanroom and shell profiles (Fig. 3a(12)); this consisted in 2–3 mm-thick PVC flooring, bonded to the wood slab by using adhesive glue.

The ceiling system was walkable and included lighting and ventilation system. In particular, two lights were integrated in the ceiling, as well as supply and recovery ventilation ports. The finish level of the ceiling corresponded to 2.8 m height (from cleanroom flooring), at a level lower than the height of the partition system. The components of the ceiling diaphragm included extruded aluminum 6060-T5 elements: T-shape profiles (Fig. 3b(1)),

angular joint connectors (Fig. 3b(2)), loadbearing panels (Fig. 3b(3)), H-shaped profiles (Fig. 2b(7)), stiffened suspension connection profile elements (Fig. 3b(4)), angular profile elements (Fig. 2a(3)).

The ceiling hanger-suspension devices consisted in six threaded rods (Fig. 3b(5)) integrated with hinges (at the extremities) (Fig. 3b(6)) and spring devices (in the internal part) (Fig. 3b(7)); the extremities of the suspension devices were fastened to the test frame (superiorly) and to the ceiling diaphragm (inferiorly, to the stiffened suspension connection profile elements) after the ceiling diaphragm was assembled. The hinge devices allowed rotation along both horizontal directions, whereas spring devices allowed elongation of the suspension devices (horizontal displacements of the ceiling system), minimizing the suspension reactions associated with axial deformation of the rods; the spring devices consisted in a series of two spring elements (Fig. 3b(7)), designed according to maximum expected seismic demand deformations. The lighting system, consisting in two lights, and the ventilation system, consisting in airflow supply and recovery ports, were integrated within the panels after their assembly.

T-shape profiles defined the perimetrical support of the ceiling system over the lateral partition system and were screw fastened to the vertical panels (Fig. 3b(8) and (9)); adjacent perpendicular T-shape profiles were connected through angular joint connectors. Loadbearing panels were placed on and fixed to the T-shape profiles along north–south direction; H-shaped profiles were used to screw fasten adjacent panels, they were inserted within the panel-to-panel gaps (Fig. 3b(10)) and the panels were screwed to them; stiffened suspension connection profile elements were inserted within panel-to-panel profile connections (Fig. 3b(10)) and superiorly screw fastened to the panels and the H-shaped profiles (Fig. 3b(11)), to also strengthen the panel-to-panel connection. Superiorly to the panels, angular profile elements were screwed to both ceiling panels and vertical panels along the perimeter of the ceiling system (Fig. 3b(12)). Figure 4 depicts the assembled ceiling system from (a) the top and (b) the inside of the cleanroom.

2.3 Innovative technologies

As was previously discussed, the innovative cleanroom was provided with advanced technological devices specifically designed to improve seismic performance and

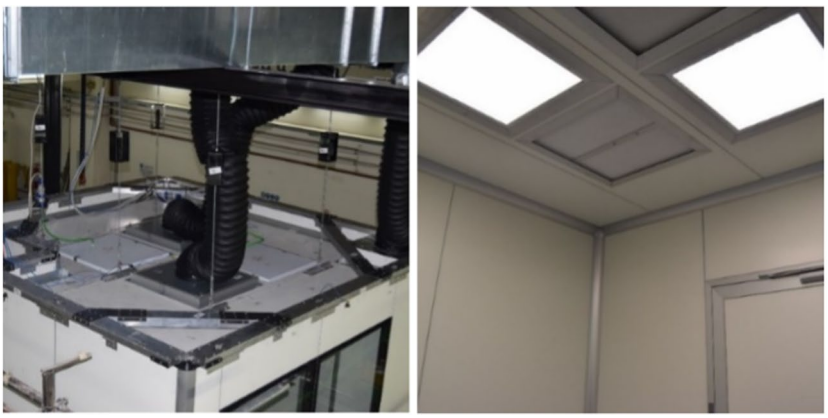

Fig. 4 View of the assembled ceiling system: **a** from the top and **b** from the inside the cleanroom

efficiency of the system (e.g., for industrial optimization purposes). In fact, traditional cleanrooms are generally not designed against seismic forces. A force-based seismic design approach was implemented, with the highest seismic hazard in Italy for critical buildings as reference and with the aim to satisfy operativity limit state (OLS) and life safety limit state (LSLS) according to the Italian (Ministero delle Infrastrutture e dei Trasporti 2018, 2019) and European seismic codes (British Standards Institution and European Committee for Standardization 2005). All cleanroom components, including the innovative ones, were described in the previous section and the innovative nature of the components was claimed. However, a focus on the technological devices is given in this section, and the main cleanroom innovative devices are described below, referring to the complete description reported in Sect. 2.2.

- Bottom splice (Fig. 2a(4)); this device implements a mechanical node connection among (a) cleanroom supporting floor, (b) (adjacent perpendicular) base profiles, (c) (adjacent perpendicular) lateral panels bottom part, (d) (vertical) curved angular profiles and vertical threaded rod; this connection is relatively rigid, rapidly installable, and fully reversible; the splice geometrical characteristics were defined to maximize the efficiency.
- Top splice (Fig. 2b(9)); this device, similarly to the bottom splice, implements a mechanical node connection among (a) (adjacent perpendicular) top profiles, (b) (adjacent perpendicular) lateral panels top part, (c) (d) (vertical) curved angular profiles and vertical threaded rod; as the bottom splice, this connection is relatively rigid, rapidly installable, and fully reversible, as well as the its geometry maximizes the efficiency.
- Bottom block (Fig. 2a(5)); this device has functions and characteristics similar to the bottom and top splices but it implements the mechanical node connection at adjacent parallel panels; furthermore, this device prevent the overturning of the panels since it is inserted within the slot of a telescopic track, fixed with a clamp and bolted to the vertical splice that connects the adjacent panels.
- T profile (Fig. 2b(11)); this device implements a mechanical connection between adjacent parallel panels, fastening their upper adjacent corners; two longitudinally adjacent T profiles are implemented for each connection, one at each side of the panels; the adjacent T profiles define a slot that is crossed by the vertical splice; T profiles are laterally screwed to the panels and vertically screwed to the top frame element.
- Upper perimetrical RHS profile (Fig. 2b(10)); this profile was installed along the upper perimeter of the cleanroom top (above the panels) and it was fastened to the top splice devices; this device implemented a relatively rigid and continue restrain action at the top of the cleanroom panels.
- Horizontal brace (Fig. 2b(12)); this device implements a rigid node at the top corner between adjacent perpendicular panels; in particular, the connection is made by a diagonal corner profile connected to the two adjacent perpendicular perimetrical profiles elements by 45° plate braces, screwed to the frame and diagonal profiles.
- Ceiling suspension device (Fig. 3b(4)–(7)); this system is composed of multiple components, including hanger threaded rods integrated with hinges at their extremities and equipped with spring devices; due to the hinges (allowing for almost free end rotation) and the springs (with a high elongation capacity), a significant amount of relative displacement is allowed within the ceiling system; as a result, the ceiling can become uncoupled from the upper story that supports it.

- Shock absorber (Fig. 3a(5)); this device was inserted between the floor rail profiles and the transparent-blind panels to minimize the damage to the glass panels in case of seismic actions.

2.4 Monitoring instrumentation

Monitoring instrumentation consisted of eleven accelerometers (Acc), eight displacement laser sensors (Las), four wire potentiometers (WPot), and four video cameras (Fig. 5a). The accelerometers were three-axis piezoelectric devices, with a measurement range of ± 10 g and a sampling rate of 100 Hz. Four accelerometers (Acc662, Acc766, Acc050, and Acc053) were positioned at the middle of the lateral panels of the cleanroom, on the outer side. Three accelerometers (Acc763, Acc818, and Acc054) were located at the top of the lateral panels (middle width), corresponding to south, east, and west side panels; an additional accelerometer (Acc765) was installed on the west side panel, corresponding to the bottom of the lateral panel (middle width). An accelerometer (Acc762) was installed on the wood slab (middle width), corresponding to the west side. Two accelerometers (Acc052

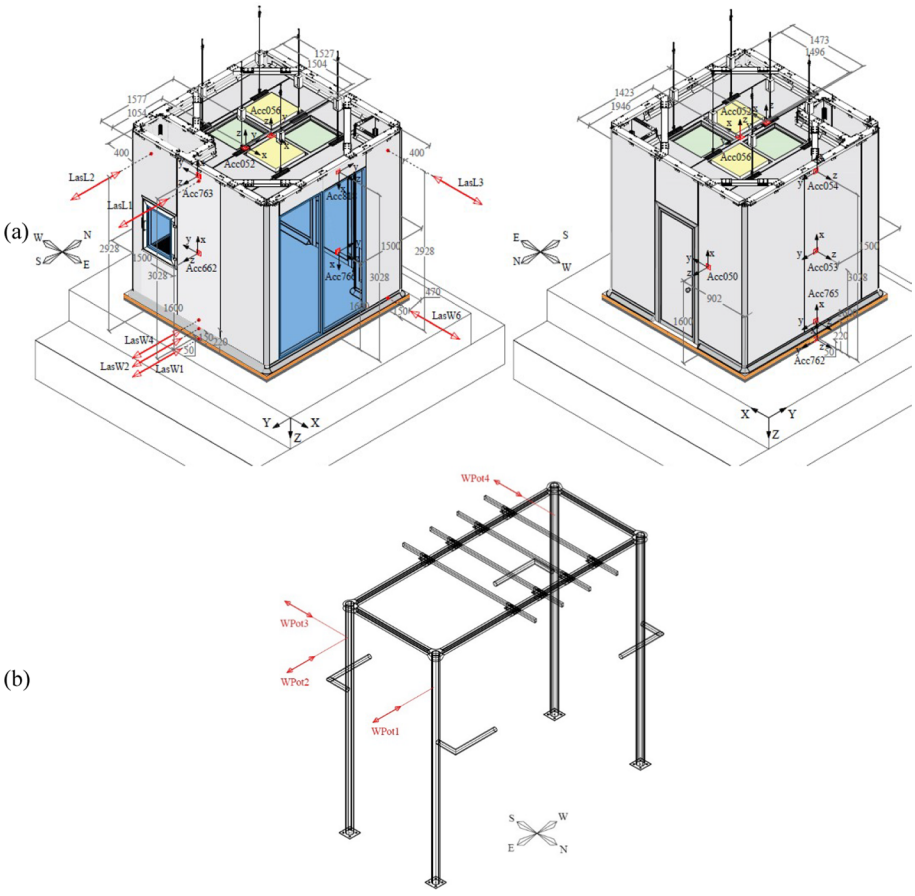

Fig. 5 Perspective view of the instrumentation arrangement: **a** specimen and **b** test frame

and Acc056) were placed on the ceiling system, corresponding to suspension connection element and panel frame.

The shake table was monitored by internal accelerometers (AccTX and AccTY, not depicted in Fig. 5a). "Luchsinger" e "Wenglor" type laser sensors were used (LasL and LasW, respectively); the former (latter) had a measurement range of 600 (200) mm at high resolution equal to 80 µm (50 µm); both sensor types are unaffected by materials, colors, and brightness issues.

Five laser sensors were installed on the south side (LasL1, LasL2, LasW1, LasW2, and LasW4) and two on the east side (LasL3 and LasW6); displacement of the shake table along X and Y direction were monitored by LasW3 and LasW5, respectively (not depicted in Fig. 5a). LasL (LasW) sensors were 400 (250) mm distant from the specimen. The top displacements of the test frame were monitored by four wire potentiometers (WPot1, WPot2, WPot3, and WPot4, Fig. 5b); WPot1, WPot2, and WPot3 (WPot 4) had a measurement range equal to 300 (150) mm. The pressure within the cleanroom was monitored in real time by means of air pressure sensors with accuracy of up to ± 0.5 Pa and measurement of minimal differential pressures from 0 to 50 Pa, according to UNI EN ISO 14644-3 (European Committee for Standardization (CEN) 2019), considering ISO Class 7 requirements (European Committee for Standardization (CEN) 2021; Yang et al. 2021). In particular, a differential pressure transducer connected externally to the control unit was installed inside the cleanroom.

2.5 Testing procedure and loading inputs

Both dynamic identification and seismic performance evaluation tests were carried out through mono- and bi-directional shake table testing, respectively (Zito et al. 2022b). Dynamic identification tests (RAN tests) were performed considering 60-s low-amplitude random vibration signals (Di Sarno et al. 2015) (i.e., maximum acceleration not exceeding 0.2 g), which were obtained by a uniform random stationary process (Clough and Penzien 2003). The shake table input to perform seismic performance evaluation tests was developed according to the ICC-ES AC156 protocol (International Code Council Evaluation Service (ICC-ES) 2020). This protocol is among the most used in both practice and literature applications (Zito et al. 2022b). The procedure implemented to generate the signal can be found in (Magliulo et al. 2012) regarding AC156 and in Zito et al. (2022a) considering an alternative protocol. Seismic performance evaluation tests were carried out through incremental tests (AC tests), by scaling the reference seismic input up to peak table accelerations larger than 2 g. Dynamic identification tests were performed prior to and after the incremental procedure, and in-between all incremental steps; this was aimed at assessing the correlation between the damage and the dynamic property evolution (e.g., Di Sarno et al. 2015; Gaviria and Montejo 2019). Design spectral acceleration at short periods S_{DS} was used as a reference intensity measure for scaling the intensity of the incremental tests. Figure 6 shows (a) acceleration time history and (b) response spectra associated with the reference seismic inputs along both horizontal directions considering S_{DS} equal to 1.50 g. In particular, test response spectra (TRS) and required response spectra (RRS) are depicted in Fig. 6b, considering one-sixth-octave bandwidth resolution along the ordinate axis.

Table 1 reports the loading program (RAN and AC tests (bold and underlined)), maximum corresponding accelerations recorded on shake table (PFAt) and wood slab (PFAs)) along horizontal directions, and percentage variation (V). RAN100i (RAN200i) corresponds to unidirectional tests along X (Y) direction.

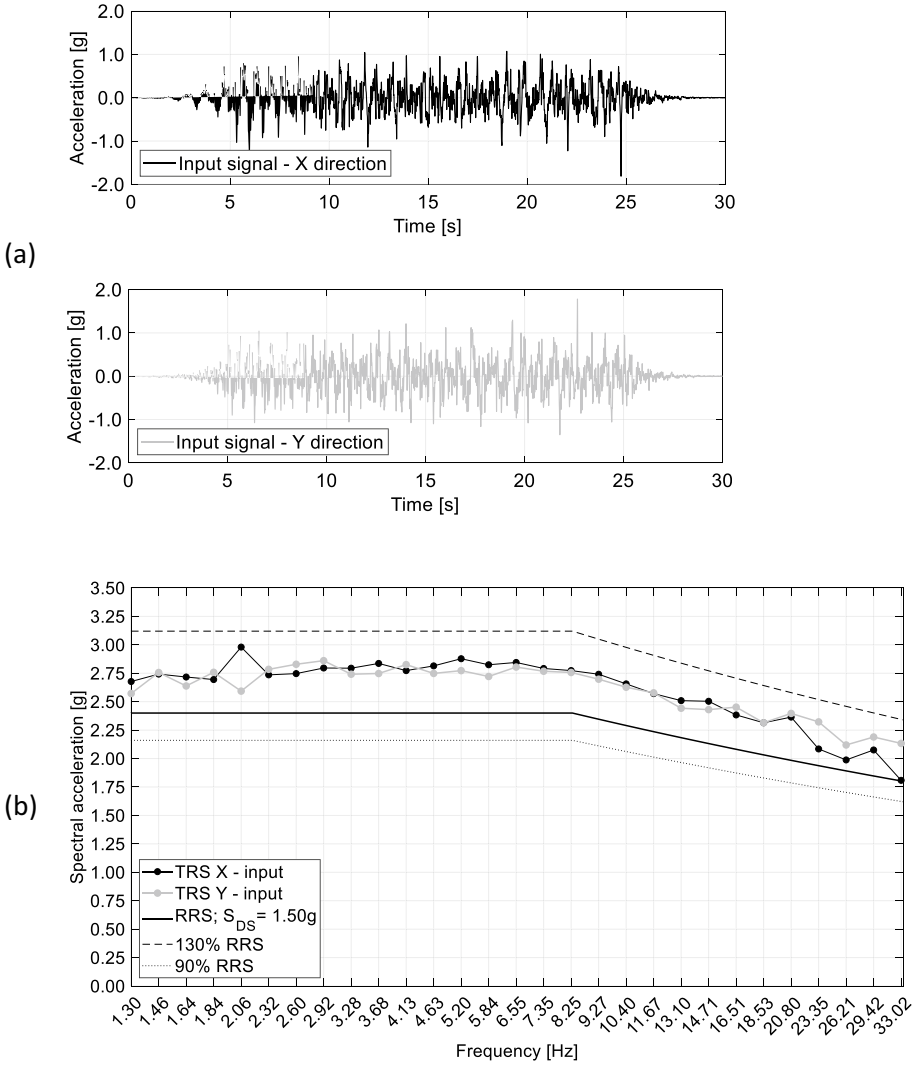

Fig. 6 AC156 testing input corresponding to S_{DS} equal to 1.50 g: **a** acceleration time histories and **b** acceleration response spectra (i.e., test response spectra (TRS) and required response spectra (RRS))

2.6 Dynamic identification

The dynamic properties of the cleanroom were assessed by using the transfer function method (Clough and Penzien 2003). In particular, the transfer curves and associated vibration modes of the specimen were assessed considering RAN tests; the modes are only qualitative discussed in the paper. The natural frequencies (local peak frequencies) and damping ratios were estimated, and their evolution along the incremental tests was assessed. The transfer functions were defined as the ratio of the Fourier transforms related to acceleration time histories recorded at the cleanroom top and on the shake table. Acc054z and Acc054y

Table 1 Testing program, maximum accelerations recorded on shake table (PFA_t) and wood slab (PFA_s), and (V) percentage variation

Test ID	S_{DS} [g]	PFA_{tx} [g]	PFA_{ty} [g]	PFA_{sx} [g]	PFA_{sy} [g]	V_x [%]	V_y [%]
RAN1000	–	0.20	–	–	–	–	–
RAN2000	–	–	0.20	–	–	–	–
AC01	**0.10**	**0.12**	**0.11**	**0.12**	**0.11**	**–0.60**	**–1.20**
AC02	**0.20**	**0.25**	**0.25**	**0.25**	**0.25**	**0.10**	**0.80**
AC03	**0.30**	**0.38**	**0.37**	**0.38**	**0.37**	**–0.50**	**0.90**
AC04	**0.40**	**0.50**	**0.48**	**0.50**	**0.48**	**–0.20**	**0.00**
RAN1003	–	0.20	–	–	–	–	–
RAN2003	–	–	0.20	–	–	–	–
AC05	**0.50**	**0.64**	**0.58**	**0.62**	**0.58**	**–2.00**	**–0.10**
RAN1004	–	0.20	–	–	–	–	–
RAN2004	–	–	0.20	–	–	–	–
AC06	**0.60**	**0.75**	**0.64**	**0.74**	**0.64**	**–1.00**	**–1.50**
AC07	**0.70**	**0.85**	**0.76**	**0.86**	**0.75**	**1.00**	**–1.50**
AC08	**0.80**	**1.01**	**0.85**	**0.99**	**0.86**	**–2.40**	**1.50**
RAN1007	–	0.20	–	–	–	–	–
RAN2007	–	–	0.20	–	–	–	–
AC09	**0.90**	**1.09**	**1.03**	**1.13**	**1.03**	**3.90**	**0.30**
RAN1008	–	0.20	–	–	–	–	–
RAN2008	–	–	0.20	–	–	–	–
AC10	**1.00**	**1.27**	**1.12**	**1.26**	**1.11**	**–0.70**	**–1.00**
RAN1009	–	0.20	–	–	–	–	–
RAN2009	–	–	0.20	–	–	–	–
AC10bis	**1.00**	**1.54**	**1.31**	**1.27**	**1.39**	**–17.40**	**6.00**
RAN1009bis	–	0.20	–	–	–	–	–
RAN2009bis	–	–	0.20	–	–	–	–
AC11	**1.10**	**1.42**	**1.51**	**1.42**	**1.61**	**–0.10**	**6.40**
RAN1010	–	0.20	–	–	–	–	–
RAN2010	–	–	0.20	–	–	–	–
AC12	**1.20**	**1.50**	**1.72**	**1.53**	**1.79**	**1.90**	**3.80**
RAN1011	–	0.20	–	–	–	–	–
RAN2011	–	–	0.20	–	–	–	–
AC13	**1.30**	**1.58**	**1.87**	**1.73**	**1.94**	**9.90**	**3.40**
RAN1012	–	0.20	–	–	–	–	–
RAN2012	–	–	0.20	–	–	–	–
AC14	**1.40**	**1.86**	**2.06**	**1.88**	**2.12**	**1.10**	**3.10**
RAN1013	–	0.20	–	–	–	–	–
RAN2013	–	–	0.20	–	–	–	–
AC15	**1.50**	**1.96**	**2.20**	**2.05**	**2.27**	**4.70**	**3.20**

(Fig. 5) were considered as output accelerometers for X and Y directions, respectively, whereas AccTX and AccTY were considered as input accelerometers.

The equivalent damping ratio associated with the first mode of the cleanroom was evaluated according to the half-power bandwidth method (Chopra 2007; Clough and Penzien

2003), typically used to assess structures and components assumed to have linear viscous damping (Di Sarno et al. 2015; Papagiannopoulos and Hatzigeorgiou 2011); it was evaluated by assessing the transfer functions obtained by RAN tests.

2.7 Seismic performance, demand, and capacity

According to performance-based earthquake engineering (PBEE) approach (Deierlein et al. 2003; Filiatrault et al. 2021; Filiatrault and Sullivan 2014; Magliulo and D'Angela 2024; Structural Engineers Association Of California (SEAOC) 1995), performance levels (PLs) are associated with limit state (LS) safety verification, which should be assessed with regard to the achievement of relevant damage states (DSs). In particular, the safety assessment should be based on the comparison of demand and capacity measures associated with the relevant LSs and DSs, respectively, and these measures should be expressed in terms of robust engineering demand parameters (EDPs). Whereas the seismic demand is defined by the relevant regulations or literature studies (e.g., British Standards Institution and European Committee for Standardization 2005; Ministero delle Infrastrutture e dei Trasporti 2018; Petrone et al. 2015; Vukobratović and Fajfar 2016), the seismic capacity should be assessed by experimental, numerical/analytical, observational, or hybrid methods (Perrone et al. 2019; Zito et al. 2022b).

PFA can be considered as a reasonable demand measure (EDP) to assess the seismic safety of the tested cleanroom. Even though the present paper does not aim to perform a seismic safety assessment, the seismic demand PFA associated with high-, medium-, and low-seismicity sites in Italy is depicted in Fig. 7 for a representativity and generality purpose. In particular, (a) L'Aquila, (b) Naples, and (c) Milan sites are considered,

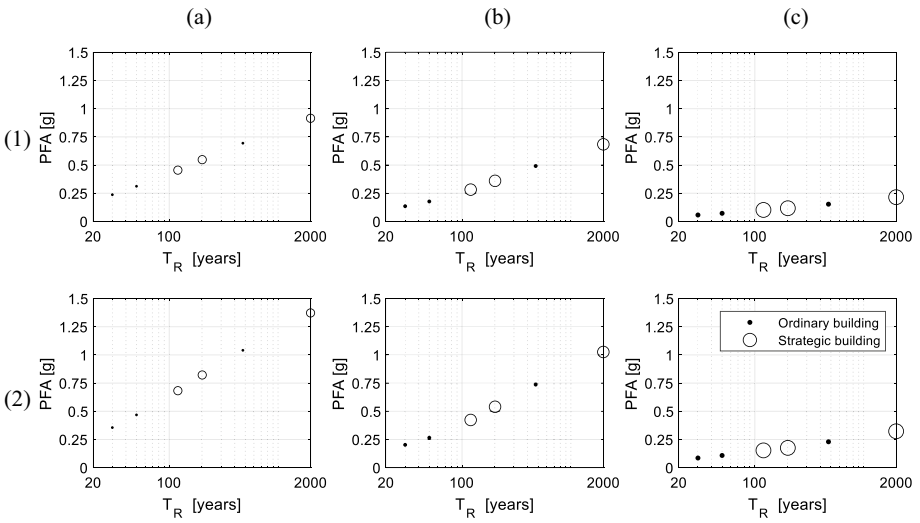

Fig. 7 Seismic demand peak floor acceleration (PFA) as a function of return period (T_R), associated with operativity limit state (OLS), damage limitation limit state (DLS), and life safety limit state (LSLS), considering both ordinary and strategical buildings, for **a** L'Aquila, **b** Naples, and **c** Milan (Ministero delle Infrastrutture e dei Trasporti 2018, 2019); (1) PFA to PGA ratio equal to 2 according to the Italian building code NTC 2018 (Ministero delle Infrastrutture e dei Trasporti 2018, 2019) and (2) PFA to PGA ratio equal to 3 according to ASCE 7-16 (American Society of Civil Engineers 2017)

and OLS, damage limitation limit state (DLS), and LSLS demand PFA are shown for both ordinary and strategical buildings, according to the Italian building code NTC 2018 (Ministero delle Infrastrutture e dei Trasporti 2018, 2019). PFA is plotted as a function of the return period (T_R) associated with the considered LSs and building class (ordinary or strategic); two PFA to PGA ratio values are assumed for the sake of completeness: (1) PFA/PGA equal to 2, according to NTC 2018, and (2) PFA/PGA equal to 3, according to ASCE 7-16 (American Society of Civil Engineers 2017). As it can be seen in Fig. 7, the maximum testing PFA (about 2.0 g) is larger than the most severe demand PFA (about 1.4 g), which corresponds to LSLS for a strategic building located in L'Aquila considering PFA to PGA ratio equal to 3.

Damage and capacity assessment was performed considering the following damage states (DSs): DS0 (no damage), DS1 (minor damage), DS2 (moderate damage), and DS3 (major damage), according to the literature (Hasani and Ryan 2021; Petrone et al. 2017). Generally, a DS can be achieved by each (significant) component of a specimen in the course of a seismic test, and, in this context, the most severe DS achieved by (at least) a component over an incremental test is meant as a global DS achieved by the specimen from that increment on. DS1 achievement implies the need to implement minor repair/rearrangement actions restoring the original conditions (of the component). Typically, achievement of DS1 is associated with violation of full operativity conditions, especially for cases in which minor damage can affect the functioning of the facility, e.g., hospitals and medical equipment. DS2 achievement implies that the component is moderately damaged so that it needs to be partially replaced or moderately repaired/rearranged. DS3 implies that the damage level is such that (a) the component needs to be totally replaced or heavily repaired/rearranged and/or (b) life safety is not ensured.

The quantitative technical correlation scheme that associates the exhibited/expected physical damage/response of the components/specimen to the DS occurrence (namely, *damage scheme*) is typically based on the damage/response significance expressed in terms of three "D" losses contributions (Federal Emergency Management Agency (FEMA) 2012), i.e., human casualties (*Deaths*), direct economic loss due to the repair or replacement of the NEs (*Dollars*), and occupancy or service loss (*Downtime*).

The damage scheme implemented in this study is reported in Table 2; this was assessed according to current practice and past studies (Petrone et al. 2017). It is worth noting that the inside-to-outside cleanroom differential pressure is a key parameter regarding the functioning of cleanroom environments. In particular, a differential pressure lowering below a threshold limit, associated with residual conditions after seismic excitation, is considered as a sufficient condition for achieving DS1.

The assumed target differential pressure within the cleanroom was set equal to 40 Pa, whereas the required minimum value was set equal to 25 Pa (European Committee for Standardization (CEN) 2021; Yang et al. 2021). Seismic response and damage of the components/specimen were checked during the tests by real-time physical inspections and recorded data observation, including the real-time monitoring of both peak and residual differential pressure over the tests. These real-time assessment results were collected from prearranged damage surveys sheets. The survey sheets were checked in the data analysis and elaboration phases, referring to video/picture and instrumental data recording. Finally, the achievement of the relevant DSs was identified according to Table 2.

Table 2 Damage scheme for the correlation between the recorded damage in each component of the cleanroom and the achieved damage state (DS)

Damage type	Need to repair or replace a percentage of components larger than		
Dollars	10%	30%	50%
Downtime	–	Moderate (1–2 days)	Significant (≥ 3 days)
Death	–	Limited	Significant
Components	DS1	DS2	DS3
Ceiling System	Localized damage to some panels	Damage to the panels and slight/moderate damage to the connection, plasticization of the spring of the hanger, slight/moderate damage to the wall trim	Fall of the panels and serious damage to the connection, breakage of the spring of the hanger, severe damage and total detachment of the wall trim
Steel panels	Slight rotation out of the plane or in the plane of the panel, sealant de-bonding	Out-of-plane rotation of the panel, local plastic strains	Overturning of the panel, widespread plastic strains
Glass panels	Slight rotation out of the plane or in the plane of the panel, sealant de-bonding	Out-of-plane rotation of the panel, cracking and local disconnections, shock absorber detachment or damage	Overturning of the panel, severe or widespread cracking
T-profile, 45° and T plate	Minor/moderate damage	Severe damage and total detachment	–
Screws	Unscrewing/failure of 10% of the screws	Unscrewing/failure of 30% of the screws	Unscrewing/failure of 50% of the screws
Mechanical fasteners for use in wood slab, L-profile, shell profile	Detachment of the shell profile (external detachment), slight damage of the L-profile	Moderate damage of the L-profile	Pull-out of the wood slab screws, severe damage and total detachment of the L-profile
Angle and vertical splice profile	Slight damage to the splice and its connections	Moderate damage to the splice and its connections	Severe damage/collapse of the splice and its connections
Rectangular profile, telescoping track, bottom and top edge splice, bottom block	Minor damage	Moderate damage	Severe damage and total detachment
Ventilation and electrical system	Slight damage to components such as lights, filter, system malfunction, breakage of suspension hooks, air control (< 25 Pa), slight damage to pipes and their connections	Moderate damage to light supports and filter, serious damage/collapse of pipes and their connections	Severe damage and total detachment of lights supports and filter

Table 2 (continued)

Components	DS1	DS2	DS3
Door, pass-box	Opening, minor damage to the lock, pass-box locked	Moderate damage	Severe damage, door overturning, pass-box ejection

3 Results and discussion

3.1 RRS to TRS spectrum-compatibility

The spectrum-compatibility was evaluated considering all performed tests according to AC156, assuming a one-sixth-octave bandwidth resolution and damping value equal to 5% of critical damping. Spectrum-compatibility was checked for input theoretical signals (i.e., assigned to the table) and for signals recorded on (a) shake table (AccTX and AccTY) and (b) wood slab (Acc762) along both directions. Spectrum-compatibility was verified in all cases, and representative results are depicted in Fig. 8, corresponding to (a) AC04 (S_{DS} equal to 0.40 g) and (c) AC15 (S_{DS} equal to 1.50 g) tests along (1) X and (2) Y directions; TRS and RRS are test response spectra and required response spectra, respectively. In particular, even in the very few cases in which TRS fall below RRS (e.g., Fig. 8b(2), corresponding to a frequency equal to 9.27 Hz), the compatibility is confirmed since (a) TRS ordinate is not lower than 90% RRS ordinate and (b) adjacent one-sixth-octave points ordinates are at least equal to RRS ones. In some cases, TRS exceed RRS by more than 30 percent (e.g., Fig. 8a(1), corresponding to frequencies equal to 9.27 and 10.40 Hz), not following the code recommendations. However, TRS upper limitation can be considered to be a desired condition rather than a strict

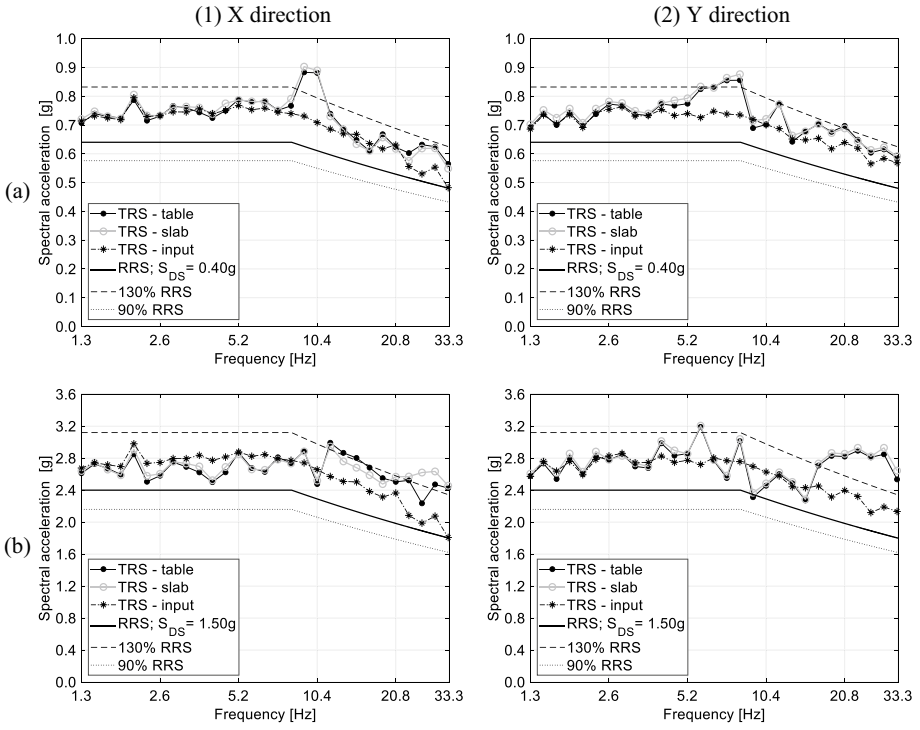

Fig. 8 Spectrum-compatibility results: required response spectra (RRS) and test response spectra (TRS) along (1) X and (2) Y directions. The results are related to tests **a** AC04 (S_{DS} equal to 0.40 g) and **b** AC15 (S_{DS} equal to 1.50 g). TRS—table, TRS—slab, and TRS—input correspond to TRS associated with records on table, records on wood slab, and input (theoretical) signal

requirement, since higher spectral ordinates are associated with higher acceleration demand severity.

3.2 Observed damage and critical response

No damage or critical response of the cleanroom was observed over all tests except for AC10 test. In fact, the opening of the doors of the pass-box was observed in the course of this latter test, resulting in a sudden drop (to zero) of differential pressure within the cleanroom, below the required minimum threshold. In particular, Fig. 9 shows the evolution of the cleanroom differential pressure over the incremental tests, where both recorded initial and recorded minimum (shaking and post-shaking) pressure values are reported, together with target and required minimum thresholds. It is recalled that the differential pressure should be larger than or equal to a required minimum value (25 Pa) to guarantee the facility operativity (DS0) (Table 2).

In all cases, initial differential pressure was within 37–40 Pa, whereas the minimum value of shaking pressure was typically between 30 and 35 MPa, except for AC10 test (as previously described). It should be noted that the post-shaking differential pressure was always larger than the recorded minimum one, reaching values similar to the initial pressures. It should be specified that more efficient correlations between the differential pressure thresholds and the damage states should be defined by the regulation/codes to carry out a more consistent performance assessment, depending on the relevant requirements.

The opening of the doors was caused by the functioning disruption of the locks; this was probably due to the demagnetization of the lock components caused by the dynamic excitation of the metal powder particles deposited within the pass-box profiles/components; this potential cause was also supported by the expert electricians of the manufacturer. After AC10 test, the lock was repaired and the functioning was fully restored (Fig. 10), and test AC10 was repeated (AC10bis).

The lock restoration consisted in (a) cleaning the slot of the lock device of the residual metallic powder and (b) reassembling the lock device; it took less than 10 min. No functioning disruption was observed (e.g., pass-box window opening did not occur); the repetition of test AC10 was associated with a similar response of the cleanroom. As previously mentioned, there is evidence suggesting that the lock failure was associated with electromagnetic and with the effect of the dynamic actions on the metallic powder located

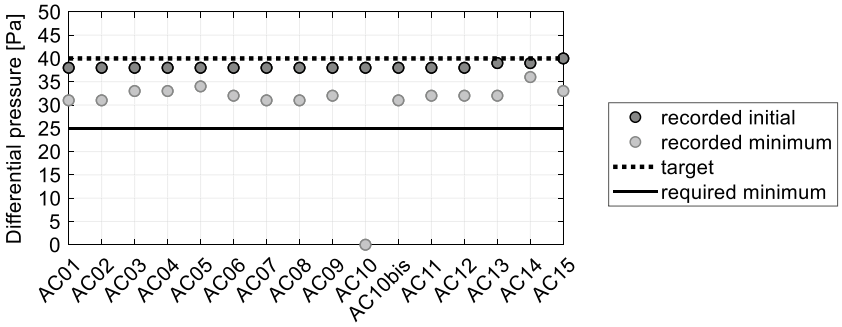

Fig. 9 Differential pressure recorded within cleanroom related to seismic performance (AC) tests: recorded initial, recorded minimum (shaking and post-shaking), target, and required minimum values

Fig. 10 Damage of the electromagnetic lock of the inside door of pass-box, ID 110 test

in the slot of the lock. After this slot has been cleared of this powder and the lock has been restored (by simple reinstatement of the lock), no lock failure occurred under the same record of AC10 test (AC10bis) as well as under significantly higher seismic actions (AC11–AC15 tests). Therefore, it can be assumed that the action of cleaning the lock slot (from the residual work powder) assures the functioning of the devices under significantly high seismic actions.

No damage or critical response (including electric/electronic issues) was observed for the following tests. Strictly speaking, the response observed in AC10 test should be associated with DS1, whereas all other test responses should be associated with DS0 (i.e., full operativity). However, test AC10, or more generally, seismic intensity related to tests AC10, might be associated with DS0. In fact, the test was repeated (AC10bis) and no damage or critical response of the cleanroom components (including pass-box windows) was identified. Moreover, the opening of the doors was more associated with an electromagnetic issue rather than to a structural behavior. Having said that, the evidence stressed the need for further investigation into the response of metal electronic locks under dynamic actions, behind the structural performance.

3.3 Dynamic identification

Figure 11 shows the dynamic identification results: (a) transfer functions (RAN test functions) and (b) peaks of the first fundamental vibration mode associated with (1) X and (2) Y directions. The transfer functions associated with the different tests are very similar among them along both directions, in terms of both peak frequencies and peak amplitudes; this strengthens the robustness of the methodology. Over a reasonably significant frequency range (0 to 35 Hz), three main relatively regular vibration modes (frequency peaks) can be identified along Y direction (20.3, 21.9 and 27.9 Hz, corresponding to 4.09, 3.33 and 2.45 amplitudes, respectively; Fig. 11a(2)), whereas the frequency response is more complex along X direction. In particular, the lowest frequency mode exhibited peak frequency (10.9 Hz) with an amplitude ordinate (1.71) significantly lower than the larger frequency mode amplitude (4.54) (Fig. 11a(1)). This evidence suggests the presence of a vibration mode (along X direction) associated with a frequency lower than the fundamental one. However, this mode is related to relatively lower ordinates and reduced dynamic significance.

The authors believe that the spectral component amplification associated with this frequency does not have a particular physical meaning. The abovementioned significantly

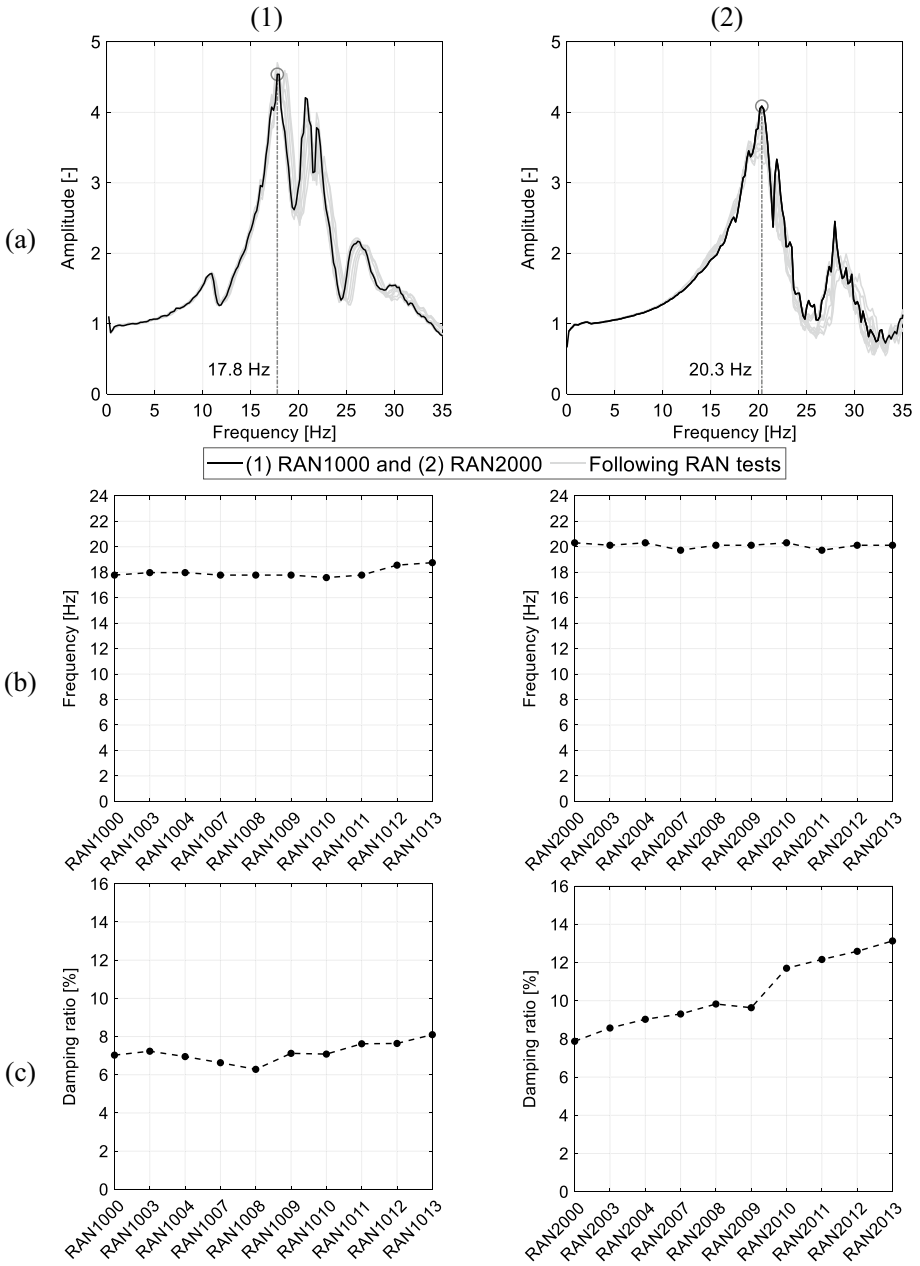

Fig. 11 Dynamic identification results (RAN tests): **a** transfer functions amplitude, **b** evolution of first vibration mode frequency peaks, **c** evolution of damping ratio of first vibration mode, along (1) X and (2) Y directions

larger response amplitude is associated with the fundamental vibration mode (17.8 Hz); other peaks along X direction are observed at 20.7, 21.9 and 26.2 Hz, corresponding to amplitudes 4.21, 3.78 and 2.17, respectively. The frequencies associated with peak

response related to X direction are lower than the corresponding ones along Y direction, showing that in the latter direction the cleanroom stiffness might be larger.

The fundamental peak frequency does not essentially vary over the incremental tests along both directions, as it can be seen in Fig. 11b (RAN tests were performed prior to and after each incremental test). Accordingly, it might be derived that the main elastic properties of the system (including the connections) are not conditioned by the effects of the incremental testing procedure, which are necessarily not associated with damage or degradation of the specimen parts. The very minor peak frequency variations identified along both directions (along X direction, maximum positive (negative) variation for following tests equal to 4.40% (−1.10%) and total variation equal to 5.49%, and along Y direction, maximum positive (negative) variation for following tests equal to 1.98% (−2.88%) and total variation equal to −0.96%) are reasonably due to very minor rearrangements among parts and connections (e.g., bolt connection loosening or sealing adjustment), which do not sensibly affect the properties of the cleanroom. The natural frequency of the cleanroom associated with undamaged conditions was equal to 17.8 (20.3) Hz along X (Y) direction, i.e., RAN1000 (RAN2000) test curve in Fig. 11a(1) (Fig. 11a(2)).

Figure 11c depicts the evolution of damping ratio of first vibration mode along RAN tests, along (1) X and (2) Y directions. The initial damping ratio (associated with RAN1000 and RAN2000 tests along X and Y direction, respectively) is quite similar for X and Y directions (equal to 7.03% and 7.87%, respectively). Damping ratio in X direction does not significantly vary along incremental tests (maximum positive (negative) variation for following tests equal to 13.3% (−5.21%) and total variation equal to 15.3%), whereas ratio in Y direction gradually increases as the test intensity grows (maximum positive (negative) variation for following tests equal to 21.5% (−1.97%) and total variation equal to 66.7%). This latter response might be due to the slight variation of the specimen connections' arrangements, which increase their damping capacity as the testing intensity increases. The estimated damping ratios are consistent with values assessed in the literature for similar components (Di Sarno et al. 2015; Fiorino et al. 2019; Petrone et al. 2017), even though it is not possible to make quantitative comparisons given the unicity of the tested specimen. Since no permanent damage was observed during the tests and at the specimen unmounting, it can be reasonably assumed that the variations observed in terms of damping are due to the variation of the arrangement/interfaces/interactions of the intra- and inter-connection components.

It should be noted that the cleanroom consists in the assembly of multiple components, implemented by means of non-standard connections, according to nonsymmetrical layouts and peculiar arrangements. The lateral partition sides are different among them and include various elements and parts in addition to the metal panels (e.g., transparent panels, pass-box, door). This geometrical and assembly complexity is necessarily associated with a complex and relatively irregular dynamic response, even considering the elastic vibration properties. For example, several sources of energy dissipation and damping are likely to affect the response of the specimens, which are mostly related to the inter- and intra-connection responses and rearrangement of the assembly. Therefore, the dynamic identification results previously reported should be interpreted in the light of this complexity, recalling that the vibrational response of the cleanroom might be reasonably conditioned by both local and global modes, even according to relatively irregular patterns.

As a final comment, it should be specified that more deformable cleanroom systems might exhibit higher sensitivity to the spectral plateau frequency range associated with AC tests, and, therefore, these might present higher component amplification factors under these latter tests, which might be more compatible with the ones associated with RAN

tests. Obviously, different systems should be specifically assessed to estimate the dynamic properties (and the seismic capacity).

3.4 Acceleration response

PFA (recorded on the shake table), peak component acceleration (PCA), and component amplification factor (CAF), i.e., PCA to PFA ratio, were estimated and associated with the incremental test intensities (AC tests), as well as CAF was also estimated considering the dynamic identification tests (RAN tests). Figure 12 depicts PCA measured corresponding to (a) cleanroom top (top of lateral partition) (Acc054), (b) ceiling system (next

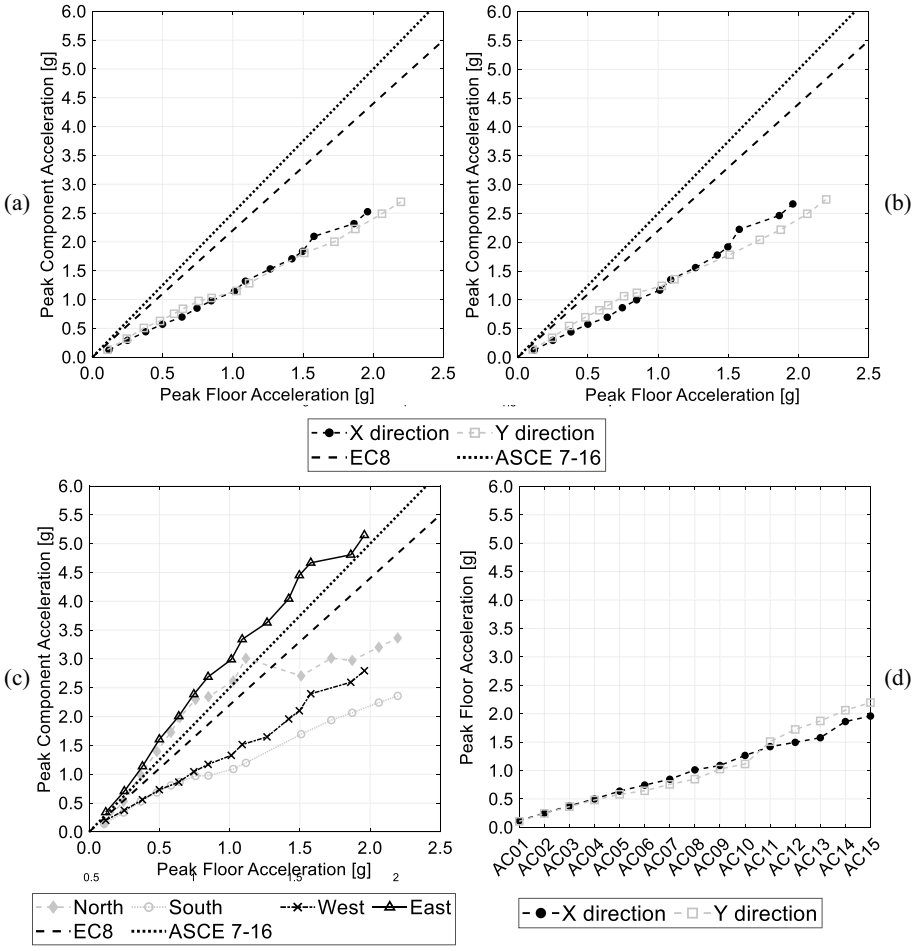

Fig. 12 Acceleration response: peak component acceleration (PCA) evolution over the incremental test peak floor acceleration (PFA) values, associated with **a** cleanroom top (lateral partition), **b** ceiling system (suspension connection), **c** lateral partition panels (out of plane directions), and **d** testing PFA. Component amplification factor (CAF), i.e., PCA to PFA ratio, provided by Eurocode 8 (British Standards Institution and European Committee for Standardization 2005) and ASCE 7-16 (American Society of Civil Engineers 2017) is depicted for comparison purposes

to the suspension connection) (Acc052), (c) lateral partition panels (out of plane direction, Acc050 (blind panel, north), Acc766 (glass panel, east), Acc662 (blind panel, south), and Acc053 (blind panel, west)), and PFA (AccTX and AccTY), along both horizontal directions.

PCA associated with cleanroom top (lateral partition) (Fig. 12a) and ceiling system (suspension connection) (Fig. 12b) are approximately the same, implying that the ceiling system is essentially rigid and rigidly connected to the lateral partition system. This is also supported by the fact that both displacement and acceleration results are compatible with no significant plane rotation of the ceiling system and no torsional effects. PCA (approximately) grows linearly as PFA increases, with very similar gradient along X and Y direction, according to testing PFA (Fig. 12d). PFA was approximately the same along X and Y direction up to AC10 test, with PFA slightly larger along X, whereas PFA along Y became larger from tests following AC10. The trend of the out of plane PCA (Fig. 12c) is more irregular than the one associated with top responses (Fig. 12a and b), especially considering north partition panel. Up to PFA equal to about 0.75 g east (west) panels PCA are almost identical to north (south) ones, whereas, for larger intensities, east (glass panel) PCA values are significantly larger than north (blind panel) ones and even larger than other panels' PCA. It should be recalled that PFA along X and Y direction presented some differences along the incremental procedure, especially for relatively large intensities, i.e., X direction PFA were slightly larger than Y ones over medium intensities and an opposite trend was observed for larger intensities (Fig. 12d). Therefore, the interpretation of PCA results should be also based on estimation of CAF. For this purpose, in Fig. 12, CAF, i.e., PCA to PFA ratios, provided by Eurocode 8 (British Standards Institution and European Committee for Standardization 2005) and ASCE 7-16 (American Society of Civil Engineers 2017) are depicted, and these are discussed in the following.

Figure 13 shows CAF related to (a) cleanroom top (Acc054), (b) ceiling system (suspension connection) (Acc052), and (c) lateral partition panels ((out of plane direction, Acc050 (blind panel, north), Acc766 (glass panel, east), Acc662 (blind panel, south), and Acc053 (blind panel, west)), and PFA (AccTX and AccTY). In particular, CAF was assessed considering (1) incremental tests and PFA as an x-axis reference and (2) dynamic identification tests and RAN test ID as an x-axis reference. As a first comment, it can be observed that CAF associated with RAN tests is quite more regular over the different tests than CAF related to incremental tests.

RAN-based CAF values are overall larger than CAF associated with incremental tests and are overall constant as the testing procedure proceeds. The out of plane response of the panels is associated with CAF values larger than global response of the cleanroom, and the former is representative of local vibration modes and response. For both incremental and RAN tests, blind panels are associated with maximum CAF values equal to about 3.0–3.5, showing a relatively large dispersion over the different panels.

Considering the glass panel, CAF values derived considering RAN tests are significantly larger than CAF values related to incremental tests, even doubling it. The CAF response observed in Fig. 13 can be referred to the type and arrangement of the monitored panels. As previously mentioned, the maximum PCA is associated with the glass panel, corresponding to the East partition side. Considering both RAN and AC tests, the amplification related to this panel is extremely large (constantly equal to about 3 and 6 corresponding to AC and RAN tests, respectively). Therefore, it can be derived that the glass panel is extremely critical in terms of acceleration amplification. Conversely, if the blind panels along South and West partition sides are considered, it can be observed that the acceleration response is significantly less amplified, if compared with the glass panel.

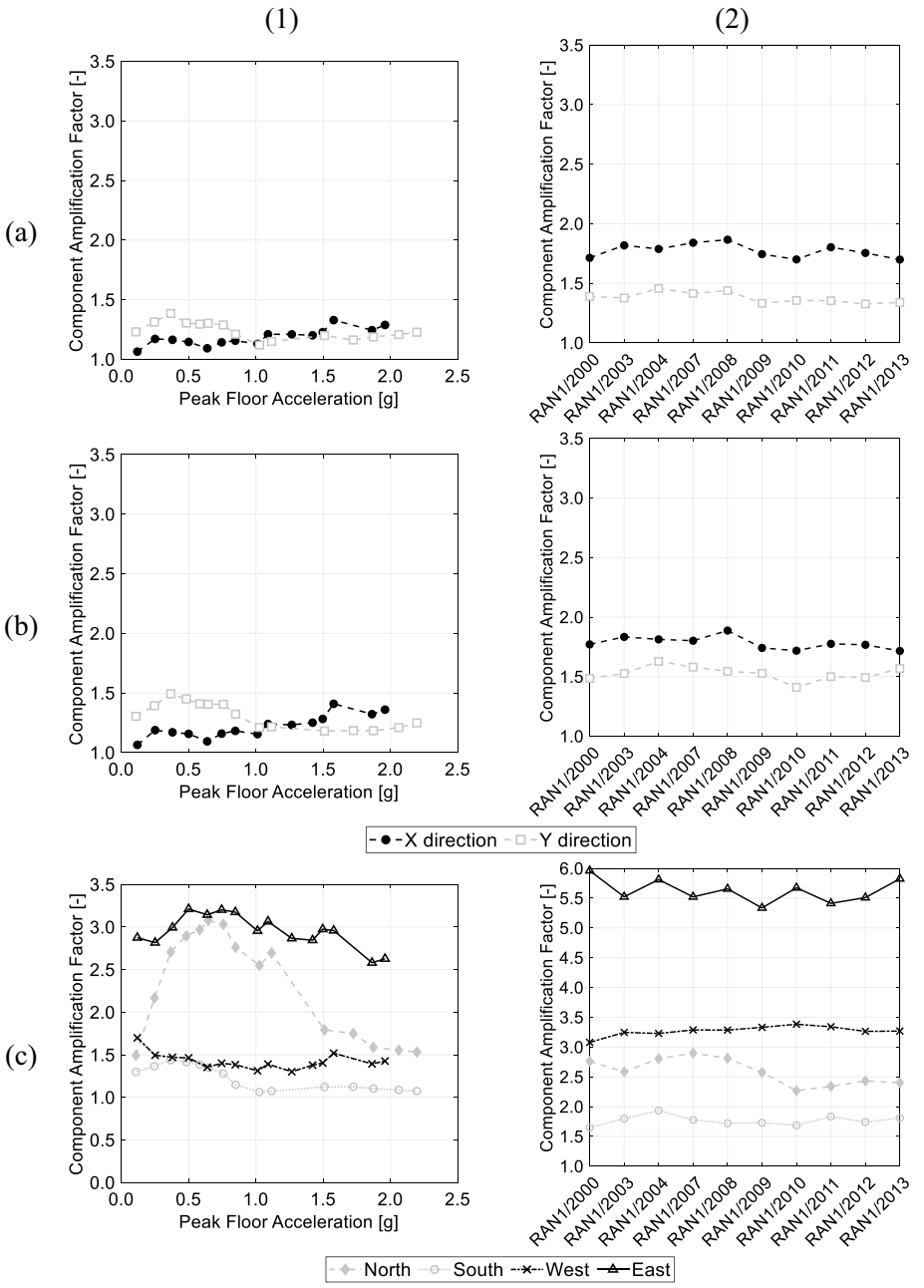

Fig. 13 Acceleration response: component amplification factor (CAF) evolution associated with **a** clean-room top (lateral partition), **b** ceiling frame (hanger-suspension device), and **c** lateral partition panels (out of plane directions), considering (1) incremental tests (AC tests), as a function of PFA, and (2) dynamic identification tests (RAN tests), as a function of RAN test IDs

In particular, considering AC tests, both panels' PCA are constantly equal to about 1–1.5, whereas, considering RAN tests, they are constantly equal to about to 3–3.5 and 1.5–2 corresponding to West and South partition sides, respectively. It is recalled that West side only includes blind panels, whereas South one includes the passbox just next to the monitored blind panel. The higher PCA associated with West side panel can be referred to the fact that the motion of the adjacent blind panels (less rigid than the passbox system) is more significant under RAN tests, if compared to the AC ones. Finally, the blind panel associated with North partition side shows a different trend considering AC tests: CAF has a maximum within 0.5–0.75 g PFA, approximately equal to 3, whereas, considering RAN tests, the response is more compatible with other blind panels ones. This behavior might be associated with the interaction between the monitored panel and the adjacent door, which seemed to be more significant over the moderate accelerations (e.g., 0.5–0.75 g PFA) and considering AC tests.

The abovementioned results stress the potential of RAN tests as a means for exciting the maximum elastic amplification response. However, this extremely amplified response might not be representative of actual amplification scenarios, i.e., associated with real or realistic seismic loading histories (e.g., Maddaloni et al. 2012; Zou et al. 2023). Accordingly, the authors would recommend assessing the acceleration amplification considering both seismic input (e.g., AC tests or other seismic records) and dynamic identification signals (e.g., RAN tests or other dynamic identification records). Furthermore, it has been found that the type of panels and their arrangement (e.g., adjacent elements) can significantly affect the acceleration amplification response. It should be noted that RAN tests cover the sensitivity frequencies of the specimens with higher spectral amplitudes, if compared to the AC tests ones. Since realistic floor motions are more compatible with AC tests rather than to RAN ones, in terms of energy and frequency contents and damage potential, the CAF associated with AC tests is reasonably more consistent than the one associated with RAN tests, as previously discussed.

Maximum CAF values related to global response of the cleanroom are not higher than typical values recommended by building codes. CAF is equal to 2.2 according to Eurocode 8 (British Standards Institution and European Committee for Standardization 2005) and, equal to 2.5, according to ASCE 7-16 (American Society of Civil Engineers 2017). For frame buildings, the Italian building code NTC 2018 (Ministero delle Infrastrutture e dei Trasporti 2018, 2019) provides CAF as a function of the building period, and this is equal to 2.5, 4, and 5 if the building period is higher than 1.0 s, between 0.5 and 1.0 s, and lower than 0.5 s, respectively. According to the experimental evidence (Figs. 12 and 13), CAF equal to 2 could be reasonably considered for accounting for the overall behavior of the cleanroom, whereas a CAF equal to 3 might be considered reliable for local design/assessment of blind panels. Larger values might be representative of the more critical response of glass panels, even though extremely large values (e.g., equal to 6) might be excessively conservative, as previously discussed. However, it should be noted that the experimental damping ratio is larger than the typical values associated with the regulation component acceleration factors (e.g., 5%). Accordingly, due attention should be paid when the experimental values are considered as a reference for design or assessment purposes.

3.5 Displacement response

Two measures of displacements are assessed under functioning conditions: (D1) relative horizontal displacement between test frame top and cleanroom top (i.e., lateral panels'

top) and (D2) relative horizontal displacement between cleanroom top (i.e., lateral panels' top) and the shake table. D1 informs regarding the transversal deformation capacity of the suspensions system and cleanroom plenum, whereas D2 is associated with the transversal deformation capacity of the cleanroom itself (including the cleanroom base to shake table interactions). Figure 14a depicts the peak values of D1, normalized considering the distance between cleanroom top and the test frame top, i.e., expressed a relative displacement ratio (namely, interstory drift ratio IDR1), as a function of the incremental test PFA values, along both directions. D1 was assessed considering the average between the two available measures, i.e., WPot1 to L3 instruments and WPot2 to L3 instruments along X direction and WPot3 to L1 instruments and WPot4 to L1 instruments along Y direction. IDR1 (Fig. 14a) increases as PFA grows following an approximately linear pattern, even though response along X direction is more regular than along Y direction. In particular, the suspensions system and cleanroom plenum were found to be more deformable along Y direction (i.e., larger IDR1 for given PFA), especially within 0.4–1.5 g; for lower and higher intensities, IDR1 is more comparable along X and Y directions. The more rigid response of the cleanroom along X direction can be explained by considering that the horizontal resisting system of the cleanroom top (e.g., ceiling diaphragm) is stiffer along X due to the passbox components, as it can be seen in Fig. 5.

The suspensions system and plenum are found to be able to accommodate extremely large relative horizontal displacements between the cleanroom top and the frame floor (e.g., up to IDR1 equal to 10%), without transferring interaction forces from the test frame to the cleanroom top, and, more importantly, without affecting the cleanroom functioning (if the anomaly related to test AC10, previously discussed, is neglected). Therefore, the cleanroom system can be assumed to be fully uncoupled from the test frame, and, generally, from the building top floor in which the cleanroom is housed.

Figure 14b depicts the peak values of D2, normalized considering the distance between shake table/cleanroom base and cleanroom top, i.e., expressed as a relative displacement ratio (namely, interstory drift ratio IDR2), as a function of the incremental test PFA values, along both directions; for the sake of completeness, Fig. 14c depicts D2. The absolute displacements for estimating D2 were obtained by double integrating acceleration time

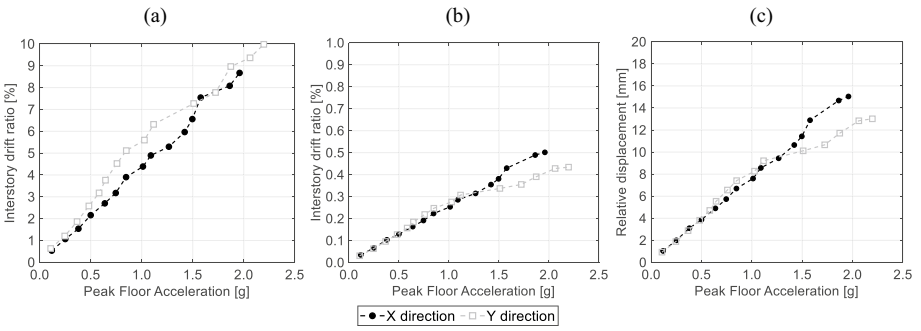

Fig. 14 Displacement response: **a** peak relative displacement between test frame story and cleanroom top (D1), normalized considering cleanroom top to test frame story distance, expressed as an interstory drift ratio (IDR1), **b** peak relative displacement between cleanroom top and cleanroom base/shake table (D2), normalized considering cleanroom height, expressed as an interstory drift ratio (IDR2), and **c** peak relative displacement between cleanroom top and cleanroom base/shake table (D2), as a function of incremental test PFA values

histories associated with the relevant accelerometers; as a matter of fact, some laser sensors went out of scale for relatively high intensities. Acc052x to AccTX instruments were considered along X direction and Acc052y to AccTY instruments along Y direction to assess the relative displacement between top of the cleanroom and the shake table, respectively. The displacements assessed through the integration of the acceleration response were found to be compatible with the displacement measured by the lasers, corresponding to the lower intensities. In particular, the difference between the two types of assessment methods was always lower than 10%.

IDR2 (Fig. 14b) linearly grows as PFA increases; the response is almost identical in X and Y direction up to about PFA equal to 1.3 g; for higher intensities, IDR2 related to X direction is larger than along Y direction. Overall, the cleanroom was found to have a relatively stiff response considering IDR2, especially if the deformability of the suspensions system and plenum of the cleanroom is considered as a reference. For example, IDR2 was lower than 0.15% (0.6%) under PFA equal to about 0.5 g (2.0 g), showing a gradient that is not affected by the test intensity (e.g., linear elastic response). It is recalled that no damage or performance/functioning disruption were observed up to the maximum intensities (if the anomaly related to test AC10, previously discussed, is neglected). Accordingly, the cleanroom system remained fully functioning up to the maximum IDR2 values.

4 Summary and conclusion remarks

The paper reported the results of an experimental campaign aimed at assessing the dynamic properties and the seismic performance of an innovative cleanroom, considering international performance requirements (ISO Class 7). The cleanroom was tested on the shake table, including the presence of a ventilation system, an electrical system, and a walkable false ceiling system. The study did not account for the vertical component of the accelerations, which might condition the response and damage of the cleanroom. In terms of deformability, it is reasonable to assume that the ceiling system is relatively rigid and that the only allowed vertical response could be associated with a limited elastic bending, limited by the vertical stiffness of the perimeter of the ceiling (constrained to the vertically stiff lateral partitions) and by the reactions of the suspension devices, acting along both tension and compression directions.

It should be claimed that the testing setup was not rigorously reproducing a realistic seismic scenario since the test frame, which supported the ceiling system, was stationary (it was fixed to the laboratory foundations). It's important to note that although the testing setup may not fully emulate realistic seismic scenarios, the study found that the ceiling response remained uncoupled from the supporting story due to the high deformation capacity and low stiffness of the suspension system. While this aspect mitigates some of the concerns regarding the testing setup, the authors acknowledge the abovementioned limitation and highlight that further investigation into more dynamic testing configurations would be beneficial for a comprehensive understanding of the seismic performance of the cleanroom.

The following main conclusion remarks can be drawn.

- The cleanroom was found to be fully operational under extremely high seismic intensities, e.g., peak floor accelerations higher than those associated with high seismicity (e.g., in Italy and Europe); it was shown that seismic demand peak floor

acceleration (PFA) related to life safety limit state (LSLS) associated with a high-seismicity Italian site and strategic buildings was lower than the highest testing PFA.
- The suspensions system-cleanroom plenum system was able to uncouple the horizontal response of the cleanroom from the test frame floor, as it was observed by assessing the relative displacement between the cleanroom ceiling and the test frame top. The study proved that the cleanroom would not be affected by extremely large potential building deformation due to seismic actions (e.g., interstory drift).
- The lateral response of the cleanroom was found to be relatively stiff, and this would preserve the functioning conditions in case of significant seismic actions. The deformation response of the cleanroom (lateral partition deformation) is relatively reduced and is not associated with damage or anomalies. This also occurs with regard to high levels of seismic actions, and it proves that the system is relatively rigid and that it can sustain high intensity actions without exhibiting damage. In particular, the maximum drift ratio associated with extremely large seismic intensities (e.g., PFA larger than 2 g) was not larger than 0.5–0.6%, which is a relatively small value if compared with the typical deformability of partitions and other architectural nonstructural elements.
- The transfer functions, fundamental frequencies, and damping ratios have been estimated. The acceleration response has been characterized in terms of time histories, peak values, and component amplification ratios, considering accelerograms recorded over several cleanroom locations/components; both peak values and amplification ratios were correlated with testing intensity. The deformability of the system has been assessed considering relative displacements, associating peak values to the testing intensity.
- Technical and constructive requirements and innovation technologic solutions are supplied for the enhancement of the seismic performance of cleanrooms. In particular, innovation components and connection arrangements are illustrated, and their efficiency is experimentally proven.
- The results of the experimental campaign cannot be easily compared with past studies since no other studies, to the authors' knowledge, investigated the seismic response of cleanrooms or complex systems similar to them. Most compatible past applications addressed seismic assessment of partition or infill walls, ceiling systems, and equipment, without integrating multiple systems and without accounting for operative facilities, as it was also discussed in the Introduction. Therefore, the present application provides significant novel knowledge and engineering solutions, importantly advancing the literature.

The study highlights the need for further studies investigating the operation of cleanrooms and other critical (building) systems integrating electric/electronic/ventilation facilities under seismic actions. Analytical and numerical methods should be developed to estimate the dynamic properties and the seismic performance of cleanroom and similar systems.

Acknowledgements The technical support of Prof. Giuseppe Maddaloni for performing the experimental tests is fully acknowledged by the authors.

Author contributions GM conceptualized the experimental tests; GM, MZ, and DD designed the test; GM, MZ, and DD carried out the test; MZ and DD elaborated the results; GM and DD validated the elaborations and optimized the data visualization; MZ and DD wrote the original draft; DD and GM revised and finalized the draft; GM supervised the project and acquired the funding.

Funding Open access funding provided by Università degli Studi di Napoli Federico II within the CRUI-CARE Agreement. This study was funded by (a) Mangini Srl, which also provided materials and assembly of the specimens, (b) the Italian Ministry of University and Research (MUR) in the framework of the national project PRIN 2020 YKY7W4 ENRICH "ENhancing the Resilience of Italian healthCare and Hospital facilities" (CUP E65F21004720001), and (c) the Italian Department of Civil Protection (DPC) in the framework of the national project DPC-ReLUIS 2022-2024 WP17 "Code contributions for nonstructural elements".

Data availability The datasets generated during and/or analysed during the current study are available from the corresponding author on reasonable request.

Declarations

Competing interests The authors have no relevant financial or non-financial interests to disclose.

References

2S.I. Software e Servizi per l'Ingegneria S.r.l. (2020) PROSAP: PROfessional Structural Analysis Program. Ferrara, Italy

American Society of Civil Engineers (2017) Minimum design loads and associated criteria for buildings and other structures, 7th edn. American Society of Civil Engineers, Reston, VA. https://doi.org/10.1061/9780784414248

Andersson AE, Bergh I, Karlsson J, Eriksson BI, Nilsson K (2012) Traffic flow in the operating room: an explorative and descriptive study on air quality during orthopedic trauma implant surgery. Am J Infect Control 40:750–755. https://doi.org/10.1016/j.ajic.2011.09.015

Arifin F, Sullivan T, Dhakal R (2020) Experimental investigation into the seismic fragility of a commercial glazing system. BNZSEE 53:144–149. https://doi.org/10.5459/bnzsee.53.3.144-149

Blasi G, Aiello MA, Maddaloni G, Pecce MR (2018) Seismic response evaluation of medical gas and fire-protection pipelines' Tee-Joints. Eng Struct 173:1039–1053. https://doi.org/10.1016/j.engstruct.2018.07.045

Braga F, Manfredi V, Masi A, Salvatori A, Vona M (2011) Performance of non-structural elements in RC buildings during the L'Aquila, 2009 earthquake. Bull Earthq Eng 9:307–324. https://doi.org/10.1007/s10518-010-9205-7

British Standards Institution, European Committee for Standardization (2005) Eurocode 8, design of structures for earthquake resistance. British Standards Institution, London

Butenweg C, Bursi OS, Paolacci F, Marinković M, Lanese I, Nardin C, Quinci G (2021) Seismic performance of an industrial multi-storey frame structure with process equipment subjected to shake table testing. Eng Struct 243:112681. https://doi.org/10.1016/j.engstruct.2021.112681

Can A, Divarci HO, Buyruk E (2021) Design principles of the hospital clean rooms. Trans FAMENA 45:59–73

Chopra AK (2007) Dynamics of structures: theory and applications to earthquake engineering, 3rd edn. Pearson/Prentice Hall, Upper Saddle River, NJ

Clough RW, Penzien J (2003) Dynamics of structures. McGraw-Hill, New York

D'Angela A, Magliulo G, Cosenza E (2022) Incremental dynamic analysis of rigid blocks subjected to ground and floor motions and shake table protocol inputs. Bull N Z Soc Earthq Eng 55:64–79. https://doi.org/10.5459/bnzsee.55.2.64-79

Deierlein GG, Krawinkler H, Cornell CA (2003) A framework for performance-based earthquake engineering

Di Sarno L, Petrone C, Magliulo G, Manfredi G (2015) Dynamic properties of typical consultation room medical components. Eng Struct 100:442–454. https://doi.org/10.1016/j.engstruct.2015.06.036

Di Sarno L, Magliulo G, D'Angela D, Cosenza E (2019) Experimental assessment of the seismic performance of hospital cabinets using shake table testing. Earthq Eng Struct Dyn 48:103–123. https://doi.org/10.1002/eqe.3127

European Commission (2010) The rules governing medicinal products in the European Union volume 4 EU guidelines for good manufacturing practice for medicinal products for human and veterinary use. Annex 1: manufacture of sterile medicinal products. Brussels, Belgium

European Committee for Standardization (CEN) (2019) ISO 14644-3:2019. Cleanrooms and associated controlled environments—part 3: test methods. Brussels, Belgium

European Committee for Standardization (CEN) (2021) ISO 14644-1:2015. Cleanrooms and associated controlled environments—part 1: classification of air cleanliness by particle concentration. Brussels, Belgium

Federal Emergency Management Agency (FEMA) (2012) Reducing the risks of nonstructural earthquake damage—a practical guide. Report No. FEMA E-74. Washington D.C., USA.

Filiatrault A, Sullivan T (2014) Performance-based seismic design of nonstructural building components: the next frontier of earthquake engineering. Earthq Eng Eng Vib 13:17–46. https://doi.org/10.1007/s11803-014-0238-9

Filiatrault A, Kuan S, Tremblay R (2004) Shake table testing of bookcase—partition wall systems. Can J Civ Eng 31:664–676. https://doi.org/10.1139/l04-031

Filiatrault A, Perrone D, Merino RJ, Calvi GM (2021) Performance-based seismic design of nonstructural building elements. J Earthq Eng 25:237–269. https://doi.org/10.1080/13632469.2018.1512910

Fiorino L, Bucciero B, Landolfo R (2019) Evaluation of seismic dynamic behaviour of drywall partitions, façades and ceilings through shake table testing. Eng Struct 180:103–123. https://doi.org/10.1016/j.engstruct.2018.11.028

Gaviria CA, Montejo LA (2019) Monitoring physical and dynamic properties of reinforced concrete structures during seismic excitations. Constr Build Mater 196:43–53. https://doi.org/10.1016/j.conbuildmat.2018.11.106

Ghalibafian H, Bhuyan GS, Ventura C, Rainer JH, Borthwick D, Stewart RPB, Zhai E (2004) Seismic behavior of flexible conductors connecting substation equipment—part II: shake table tests. IEEE Trans Power Deliv 19:1680–1687. https://doi.org/10.1109/TPWRD.2004.832387

Hasani H, Ryan KL (2021) Experimental cyclic test of reduced damage detailed drywall partition walls integrated with a timber rocking wall. J Earthq Eng. https://doi.org/10.1080/13632469.2020.1859005

Hwang J-S, Wang S-J, Huang Y-N, Chen J-F (2007) A seismic retrofit method by connecting viscous dampers for microelectronics factories. Earthq Eng Struct Dyn 36:1461–1480. https://doi.org/10.1002/eqe.689

International Code Council Evaluation Service (ICC-ES) (2020) AC156 acceptance criteria for the seismic qualification of nonstructural components. Brea, California, USA

Liu J, Zhang L, Yang J, Chen Y, Zhang X (2021) Study on pressure control and energy saving of cleanroom in purification air conditioning system. Energy Build 253:111502. https://doi.org/10.1016/j.enbuild.2021.111502

Loomans MGLC, Ludlage TBJ, van den Oever H, Molenaar PCA, Kort HSM, Joosten PHJ (2020) Experimental investigation into cleanroom contamination build-up when applying reduced ventilation and pressure hierarchy conditions as part of demand controlled filtration. Build Environ 176:106861. https://doi.org/10.1016/j.buildenv.2020.106861

Maddaloni G, Magliulo G, Cosenza E (2012) Effect of the seismic input on non-linear response of R/C building structures. Adv Struct Eng 15:1861–1877. https://doi.org/10.1260/1369-4332.15.10.1861

Magliulo G (2021) Prove Su Tavola Vibrante per l'analisi Della Prestazione Sismica Di Una Cleanroom Serie 62 Acciaio (in Italian). Dipartimento di strutture per l'Ingegneria e l'Architettura, Università degli Studi di Napoli Federico II, Naples (in Italian)

Magliulo G, D'Angela D (2024) Seismic response and capacity of inelastic acceleration-sensitive nonstructural elements subjected to building floor motions. Earthq Eng Struct Dyn. https://doi.org/10.1002/eqe.4080

Magliulo G, Pentangelo V, Maddaloni G, Capozzi V, Petrone C, Lopez P, Talamonti R, Manfredi G (2012) Shake table tests for seismic assessment of suspended continuous ceilings. Bull Earthq Eng 10:1819–1832. https://doi.org/10.1007/s10518-012-9383-6

Magliulo G, Petrone C, Capozzi V, Maddaloni G, Lopez P, Manfredi G (2014) Seismic performance evaluation of plasterboard partitions via shake table tests. Bull Earthq Eng 12:1657–1677. https://doi.org/10.1007/s10518-013-9567-8

Mangini M, Ponzio P, Magliulo G, Mirizzi F (2020) Sistema antisismico per camere bianche. 102020000003811 (in Italian)

Merino RJ, Perrone D, Nascimbene R, Filiatrault A (2023) Performance-based seismic classification of acceleration-sensitive non-structural elements. Earthq Eng Struct Dyn 52:4222–4244. https://doi.org/10.1002/eqe.3973

Ministero delle Infrastrutture e dei Trasporti (2018) D.M. del 17/01/2018—"Aggiornamento delle Norme tecniche per le Costruzioni 2018" NTC 2018 **(in Italian)**

Ministero delle Infrastrutture e dei Trasporti (2019) Circolare 21 gennaio 2019, n. 7 C.S.LL.PP. Istruzioni per l'applicazione dell'«Aggiornamento delle "Norme tecniche per le costruzioni"» di cui al decreto ministeriale 17 gennaio 2018 (in Italian)

Mulligan J, Sullivan T, Dhakal R (2020) Experimental study of the seismic performance of plasterboard partition walls with seismic gaps. BNZSEE 53:175–188. https://doi.org/10.5459/bnzsee.53.4.175-188

Papagiannopoulos GA, Hatzigeorgiou GD (2011) On the use of the half-power bandwidth method to estimate damping in building structures. Soil Dyn Earthq Eng 31:1075–1079. https://doi.org/10.1016/j.soildyn.2011.02.007

Perrone D, Filiatrault A, Peloso S, Brunesi E, Beiter C, Piccinin R (2020) Experimental seismic response evaluation of suspended piping restraint installations. Bull Earthq Eng 18:1499–1524. https://doi.org/10.1007/s10518-019-00755-5

Perrone D, Brunesi E, Decarro F, Peloso S, Filiatrault A (2019) Seismic assessment and qualification of non-structural elements in Europe: a critical review. In: 4th international workshop on the seismic performance of non-structural elements (SPONSE). Pavia, Italy. https://doi.org/10.7414/4sponse.ID.10

Petrone C, Magliulo G, Manfredi G (2015) Seismic demand on light acceleration-sensitive nonstructural components in European reinforced concrete buildings. Earthq Eng Struct Dyn 44:1203–1217. https://doi.org/10.1002/eqe.2508

Petrone C, Magliulo G, Manfredi G (2017) Shake table tests on standard and innovative temporary partition walls. Earthq Eng Struct Dyn 46:1599–1624. https://doi.org/10.1002/eqe.2872

Petruzzelli F (2016) Seismic risk assessment of an industrial plant struck by the Emilia 2012 earthquakes. IJFE 3:146. https://doi.org/10.1504/IJFE.2016.075995

Prota A, Zito M, D'Angela D, Toscano G, Ceraldi C, Fiorillo A, Magliulo G (2022) Preliminary results of shake table tests of a typical museum display case containing an art object. Adv Civ Eng 2022:1–18. https://doi.org/10.1155/2022/3975958

Shao X, Hao Y, Liang S, Wang H, Liu Y, Li X (2022) Experimental characterization of particle distribution during the process of reducing the air supply volume in an electronic industry cleanroom. J Build Eng 45:103594. https://doi.org/10.1016/j.jobe.2021.103594

Soroushian S, Maragakis E, Jenkins C (2015) Capacity evaluation of suspended ceiling components, part 1: experimental studies. J Earthq Eng 19:784–804. https://doi.org/10.1080/13632469.2014.998354

Soroushian S, Maragakis E, Ryan KL, Sato E, Sasaki T, Okazaki T, Mosqueda G (2016) Seismic simulation of an integrated ceiling-partition wall-piping system at e-defense. II: evaluation of nonstructural damage and fragilities. J Struct Eng 142:04015131. https://doi.org/10.1061/(ASCE)ST.1943-541X.0001385

Structural Engineers Association Of California (SEAOC) (1995) Vision 2000 report. Performance based seismic engineering of buildings

Taghavi S, Miranda E (2003) Response assessment of nonstructural building elements. PEER report 2003/05. (PEER report No. 2003-03.). Pacific Earthquake Engineering Research Center, University of California at Berkeley, Berkeley, California

Tian Y, Filiatrault A, Mosqueda G (2015) Seismic response of pressurized fire sprinkler piping systems I: experimental study. J Earthq Eng 19:649–673. https://doi.org/10.1080/13632469.2014.994147

Tran T-T, Cao A-T, Kim D, Chang S (2020) Seismic vulnerability of cabinet facility with tuned mass dampers subjected to high- and low-frequency earthquakes. Appl Sci 10:4850. https://doi.org/10.3390/app10144850

Vukobratović V, Fajfar P (2016) A method for the direct estimation of floor acceleration spectra for elastic and inelastic MDOF structures. Earthq Eng Struct Dyn 45:2495–2511. https://doi.org/10.1002/eqe.2779

Wittich CE, Hutchinson TC (2015) Shake table tests of stiff, unattached, asymmetric structures: shake table tests of stiff, unattached, asymmetric structures. Earthq Eng Struct Dyn 44:2425–2443. https://doi.org/10.1002/eqe.2589

Yang Z, Hao Y, Shi W, Shao X, Dong X, Cheng X, Li X, Ma X (2021) Field test of pharmaceutical cleanroom cleanliness subject to multiple disturbance factors. J Build Eng 42:103083. https://doi.org/10.1016/j.jobe.2021.103083

Yang W, Zou X, Wang M, Liu P (2023) A multinomial logistic regression model-based seismic risk assessment method for museum exhibition halls. J Build Eng 69:106312. https://doi.org/10.1016/j.jobe.2023.106312

Zhang F, Shiue A, Fan Y, Liu J, Meng H, Zhang J, Leggett G (2022) Dynamic emission rates of human activity in biological cleanrooms. Build Environ 226:109777. https://doi.org/10.1016/j.buildenv.2022.109777

Zito M, D'Angela D, Maddaloni G, Magliulo G (2022a) A shake table protocol for seismic assessment and qualification of acceleration-sensitive nonstructural elements. Comput Aided Civil Eng. https://doi.org/10.1111/mice.12951

Zito M, Nascimbene R, Dubini P, D'Angela D, Magliulo G (2022b) Experimental seismic assessment of nonstructural elements: testing protocols and novel perspectives. Buildings 12:1871. https://doi.org/10.3390/buildings12111871

Zou X, Yang W, Liu P, Wang M (2023) Floor acceleration amplification and response spectra of reinforced concrete frame structure based on shaking table tests and numerical study. Archiv Civ Mech Eng 23:156. https://doi.org/10.1007/s43452-023-00648-0